Dissecting the effect of rainfall variability on the statistical structure of peak flows

Mandapaka, Pradeep V.; Krajewski, Witold F.; Gupta, Vijay K.; Mantilla, Ricardo.

2009

Mandapaka, P. V., Krajewski, W. F., Mantilla, R., & Gupta, V. K. (2009). Dissecting the Effect of Rainfall Variability on the Statistical Structure of Peak Flows. Advances in Water Resources, 32(10), 1508–1525.

https://hdl.handle.net/10356/95606

https://doi.org/10.1016/j.advwatres.2009.07.005

Dissecting the Effect of Rainfall Variability on the Statistical Structure of Peak Flows

by

PRADEEP V. MANDAPAKA, WITOLD F. KRAJEWSKI, RICARDO MANTILLA

IIHR–Hydroscience & Engineering

The University of Iowa, Iowa City, IA 52242, USA

AND

VIJAY K. GUPTA

Civil, Environmental and Architectural Engineering

Cooperative Institute for Research in Environmental Sciences

University of Colorado, Boulder, CO 80309, USA

Corresponding author's address:

Pradeep V. Mandapaka

IIHR-Hydroscience & Engineering

The University of Iowa, Iowa City, IA 52242-1585, USA

E-mail: pmandapa@engineering.uiowa.edu

Tel: 319-594-2481

Submitted to

Advances in Water Resources

July 2009

Abstract

This study examines the role of rainfall variability on the spatial scaling structure of peak flows using the Whitewater River basin in Kansas as an illustration. Specifically, we investigate the effect of rainfall on the scatter, the scale break and the power law (peak flows vs. upstream areas) regression exponent. We illustrate why considering individual hydrographs at the outlet of a basin can lead to misleading interpretations of the effects of rainfall variability. We begin with the simple scenario of a basin receiving spatially uniform rainfall of varying intensities and durations and subsequently investigate the role of storm advection velocity, storm variability characterized by variance, spatial correlation and intermittency. Finally, we use a realistic space-time rainfall field obtained from a popular rainfall model that combines the aforementioned features. For each of these scenarios, we employ a recent formulation of flow velocity for a network of channels, assume idealized conditions of runoff generation and flow dynamics and calculate peak flow scaling exponents, which are then compared to the scaling exponent of the width function maxima. Our results show that the peak flow scaling exponent is always larger than the width function scaling exponent. The simulation scenarios are used to identify the smaller scale basins, whose response is dominated by the rainfall variability and the larger scale basins, which are driven by rainfall volume, river network aggregation and flow dynamics. The rainfall variability has a greater impact on peak flows at smaller scales. The effect of rainfall variability is reduced for larger scale basins as the river network aggregates and smoothes out the storm variability. The results obtained from simple scenarios are used to make rigorous interpretations of the peak flow scaling structure that is obtained from rainfall generated

with the space-time rainfall model and realistic rainfall fields derived from NEXRAD radar data.

1. Introduction

Peak flows in a basin are difficult to predict because they result from a complex interaction among rainfall and various processes in the landscape. Hydrology literature is rife with models developed to predict hydrographs at the outlet or at specific locations (e.g., Beven [3]; Singh and Frevert [40]; Singh and Frevert [41]). Several studies have examined the sensitivity of the hydrologic response of a basin to the spatio-temporal variability of rainfall (e.g., Krajewski et al. [22]; Ogden and Julien, [35]; Nicótina et al. [32]). However, as we illustrate with a simple simulation experiment in Section 4, examining the basin response in terms of outlet hydrograph can be misleading. On the other hand, studies have also revealed that the peak flows from a basin display power-law behavior (or scaling or scale-invariance) with respect to the drainage areas (e.g., Smith [43]; Gupta et al., [17]; Goodrich et al. [11]; Ogden and Dawdy [34]; Furey and Gupta [8]; Furey and Gupta [9]). The exponent of such a power law is widely known as the scaling exponent. Gupta et al. [19] have demonstrated that a physical understanding of the scaling behavior of the peak flows is crucial for building a unified geophysical theory of flood peaks. Such a theory would be invaluable for the prediction of peak flows, particularly in ungauged basins (e.g., Sivapalan et al., [42]).

In the past two decades, numerous simulation and data-based studies were conducted to determine the physical basis of scale-invariance (e.g., Gupta and Dawdy [15], Robinson et al. [38], Gupta et al. [18], Bloschl and Sivapalan [4] Robinson and Sivapalan [37] Menabde et al. [29], Menabde and Sivapalan [28], Ogden and Dawdy [34], Furey and Gupta [8], Furey and Gupta [9]). A general consensus emerging from these studies is

that the rainfall and the channel network topology, both shown to be scale-invariant, play key roles in determining the scaling exponents of the power laws in peak flows. While most of the aforementioned research is focused on annual peak flows, there has been a recent shift toward investigating single-event peak flows (e.g., Gupta et al. [18], Ogden and Dawdy [34], Furey and Gupta [8], Mantilla et al. [26], Furey and Gupta [9]). The physical mechanisms responsible for scale invariance can be identified in a much better manner for individual rainfall-runoff events and can be extended to annual time scales by considering multiple events in a year (e.g., Gupta et al. [19]). Also, recent studies suggest that the scaling exponents of annual peak flows are related to those of single-event peak flows (e.g., Ogden and Dawdy [34], Gupta et al. [19]). Gupta [14] and Gupta et al. [19] offer a comprehensive overview of the research pertaining to the scaling of flood peaks.

The goal of our study is to clarify the role of rainfall variability on the scaling structure of peak flows. It is well known that rainfall is highly variable in space and time and that our observational capabilities result in rainfall estimates subject to considerable uncertainties (e.g. Bras and Rodriguez-Iturbe [5]; Ciach et al. [6]). This study is limited to the effects of rainfall variability, and the effect of rainfall estimation uncertainty is therefore outside of the scope of this paper. We separate the rainfall variability into various components and study, via simulation experiments, the sensitivity of peak flow scaling structure to each of them. We then apply those results in order to understand the statistical structure of peak flows obtained using rainfall from a space-time model capable of simulating realistic rainfall events. Rigorous understanding of the role of rainfall on

the scaling structure of peak flows provides the basis for the scaling based framework to predict the peak flows from real basins.

Following the introduction, Section 2 offers definitions of some basic concepts and provides a short description of the literature related to the single-event peak flow scaling structure. In Section 3, we describe the study area, the simulation framework and relevant assumptions. Section 4 compares the hydrograph-oriented and scaling-based approaches to studying the hydrologic response of a basin. In Section 5, we show the scaling structure of peak flows obtained from an actual rainfall event measured by NEXRAD weather radar in Wichita, Kansas. Section 6 includes the presentation of the results for the basic simulation scenarios that we considered. The Peak flow scaling structure obtained using the rainfall from the space-time model is discussed in Section 7. In Section 8, we present an analysis of scatter seen in the scaling structure of peak flows, followed by additional remarks in Section 9. Section 10 summarizes and concludes the study.

2. Background

In this section, we briefly discuss key results in the literature related to the statistical structure of single event peak flows. We first provide definitions of some basic concepts and then proceed to a discussion of simulation-based and data-based studies in the literature.

2.1. Basic Concepts

The Horton ratio R_X is defined as a ratio of the averages $E[X_{\omega+1}]/E[X_\omega]$, where X_ω is a generic random field indexed by Horton order ω, a stream ordering system developed by Horton [20] and later modified by Strahler [44,45]. For instance, the field X can be the upstream areas or width function maxima or peak flows. For more details on the Horton order and the Horton ratios, please see Rodriguez-Iturbe and Rinaldo [39] and Peckham and Gupta [36].

The width function of a river network is a measure of the river network branching structure. There are basically two types of width functions: topologic and geometric. Throughout this study, we employ the topologic width function, which is defined as the number of links which are s links upstream of the outlet of the basin as a function of s (e.g., Veitzer and Gupta [47]). Under idealized conditions of runoff generation and constant flow velocity, the width function represents the response of the river network to spatially uniform instantaneous rainfall. The statistical structure of the width function and its relation to the hydrologic response of the basin has been the object of several recent studies (e.g., Veitzer and Gupta [47]; Moussa [31]; Lashermes and Foufoula-Georgiou [23]). Veitzer and Gupta [47] showed that the width function maxima of the simulated random self-similar channel networks follow distributional simple scaling. That is, the generalized Horton law in terms of probability distributions (e.g., Peckham and Gupta [36]) holds for the width function maxima, and the Horton ratios of width function maxima R_Θ and upstream areas R_A are related by a power law of the form.

$$R_{\Theta} = R_A^{\beta} \quad (1)$$

where β is the scaling exponent of the width function maxima. Similarly, the Horton ratios for the peak flow R_Q and upstream areas R_A are related by a power law

$$R_Q = R_A^{\phi} \quad (2)$$

when peak flow distributions exhibit statistical self-similarity, which has been shown to be the case under certain conditions of flow and rainfall (e.g., Mantilla [26]). The exponent Φ in equation 2 is referred to as the peak flow scaling exponent.

A scale break is defined in our study as a transition point in the log-log plot of peak flows vs drainage areas. As discussed in Sections 6 and 7, the scale break separates the smaller scale basin response dominated by the rainfall intensity from the larger scale basins, whose response is dominated by river network characteristics and flow dynamics and is therefore rainfall volume driven.

2.2. Simulation-based studies

Gupta et al. [18] was the first study to focus on the effect of rainfall and channel network on the scale-invariance of single-event peak flows from a deterministic Peano network. Using a numerical simulation framework, they showed that peak flows exhibit simple scaling for uniform rainfall, with the scaling exponent dependent on the fractal dimension of the channel network width function maxima. For spatially variable rainfall, they reported that the peak flows display multi-scaling, with the exponent being a

function of the channel network and the spatial variability of the rainfall. Troutman and Over [46] derived analytical expressions for channel networks and rainfall mass exponents for the general class of recursive replacement trees and instantaneous multifractal rainfall. Menabde et al. [29] focused on the attenuation due to storage in channel networks and its effect on the scaling exponents of peak flows from deterministic (Mandelbrot-Viscek and Peano networks) and random self-similar networks with linear routing and for spatially uniform rainfall. For the deterministic self-similar networks (SSNs), the scaling exponent of peak flows is smaller than the one predicted for the width function maxima (i.e., ignoring the attenuation due to storage in channel networks). Menabde et al. [29] also showed that for random SSN with smaller bifurcation ratios, the peak flows scale asymptotically.

To better understand and predict the scaling behavior of peak flows, Menabde and Sivapalan [28] introduced a dynamic and spatially distributed hillslope-link rainfall-runoff model based on representative elementary watershed (REW) consisting of three main components: a space-time model of rainfall, a hillslope model and a channel network model. The rainfall model can generate storms whose spatial structure is characterized by a discrete random cascade. The hillslope model partitions the rainfall into Hortonian runoff, subsurface flow and evaporation, which are assumed to be zero during periods of rainfall. They further assumed that all of the surface runoff reaches the channel instantaneously. The channel network is a deterministic Mandelbrot-Viscek network in which the hydraulic geometry properties at every link are obtained from observed empirical relationships. They investigated the effect of rainfall on the scaling structure of the peak flows, starting from a spatially uniform rainfall scenario and moving

to the individual storms based on discrete random cascade. They also extended the study to include continuous rainfall and annual flood peaks. The results from event-based simulations with spatially uniform rainfall and the rainfall based on the random cascade model demonstrated that the interplay between the catchment response time and the storm duration controls the scaling exponent of peak flows.

Mantilla et al. [26] discussed the difficulties in generalizing the scaling theory to the real networks and tested whether the random spatial variability of the real channel networks and their hydraulic geometry properties, coupled with flow dynamics, produce Hortonian scaling in peak flows. Based on the results from Veitzer and Gupta [47], the value of the scaling exponent of the network width function was computed for the 149 km^2 Walnut Gulch basin in Arizona (e.g., Goodrich et al. [12]). The runoff rates were estimated from two very small gauged sub-basins within the Walnut Gulch, assuming that rainfall was spatially uniform. For an instantaneously applied runoff rate, the system of ordinary differential equations describing the runoff dynamics was solved for three different scenarios: (a) constant velocity (b) constant Chezy and (c) spatially varying Chezy constant. They showed that the scaling exponent of peak flows is larger than the exponent of the width function maxima, which contradicted the results from the studies performed on the idealized basins, where the flow scaling exponent is always smaller than the exponent of the width function maxima. The contradiction is explained in terms of the relative roles of flow attenuation and flow aggregation in the river networks that were considered.

2.3. Data-based studies

Ogden and Dawdy [34] investigated the single-event and annual peak flows from the 21.2 km^2 Goodwin Creek watershed in Mississippi (e.g., Alonso and Bingner [1]), where the Hortonian mechanism of runoff generation is dominant. They considered 279 events for which flows were recorded at several interior gauging stations. The results showed that the peak flows follow simple scaling but the exponents vary from event to event and depend on the runoff production efficiency. The mean of scaling exponents is 0.831 with a standard deviation of 0.10. Some events are then filtered out with a threshold on the correlation coefficient (0.93) between the logarithm of peak flows and the upstream areas. The mean of scaling exponents from the 226 remaining events is equal to 0.826, with a standard deviation of 0.047 and a mean correlation coefficient of 0.98.

Furey and Gupta [8] explained this event-to-event variability in the peak flow power laws in Goodwin Creek watershed in terms of variability in the rainfall's excess depth and the duration. To understand the physical origin of the observed peak flow scaling, Furey and Gupta [9] proposed and applied a 5-step framework to the Goodwin Creek watershed. Gupta et al. [19] provided further observational evidence on scaling in single-event peak flows for the Walnut Gulch basin, Arizona. They reported two different sets of scaling exponents for smaller and larger scales with a scale break at around 1 km^2. They also noticed that for the events that cover almost the entire basin, the single-event scaling exponents are quite close to the scaling exponents of the annual flood quantiles.

All the studies discussed in this section focused on the fundamental question, "How is the peak flow scaling exponent linked to the channel network characteristics such as width function maxima and variability in the rainfall?" In the studies that addressed this

question using numerical simulations under idealized conditions, the complexity in the simulations increased from Gupta et al. [18] to Mantilla et al. [26]. The rainfall varied from spatially uniform to the complex cascade-based case, and the networks ranged from deterministic self-similar to random self-similar and actual river networks with linear and nonlinear routing mechanisms (e.g., Gupta et al. [18]; Veitzer and Gupta [47]; Troutman and Over [46]; Menabde et al. [29]; Menabde and Sivapalan [28]; Mantilla et al. [26]). In the data-based analyses (e.g., Ogden and Dawdy [34]; Furey and Gupta [8]; Gupta et al. [19], Furey and Gupta [9]), the variability in the scaling exponents was explained in terms of variability in antecedent conditions and storm characteristics. However, the smaller size of the basins (21.2 km^2 Goodwin Creek and the 149 km^2 Walnut Gulch basins) limited the range of scales available to explore the effect of rainfall variability on the peak flow scaling structure. Regardless of the approach followed, these studies enhanced our understanding of the relationship between the statistical structure of flood peaks and the characteristics of rainfall and channel network. However, we need to further understand and generalize the role that rainfall plays in the statistical structure of peak flows from actual river basins across a range of scales.

In this study, we perform a series of simulation experiments starting from a simple scenario of spatially uniform rainfall for a fixed duration and moving to a complex scenario in which the rainfall is obtained from a space-time rainfall model. We also investigate the sensitivity of the scaling behavior to linear and nonlinear channel routing mechanisms. We selected the simulation framework instead of a data-based analysis since it allows complete freedom to systematically explore various aspects of scale-invariance. Also, there are very few basins in the United States where streamflow data

necessary for rigorous scaling analyses are available. Our simulation covers a range of scales from ~0.1-1000 km^2, thus addressing the peak flow scaling for basin response times ranging from minutes to days.

3. Simulation Framework

3.1. Study Area

The Whitewater River basin (Figure 1), with an area of 1100 km^2, stretches between latitudes 37° 46'E and 38° 09'E and longitudes 96° 51'W and 97° 18'W. The river network extraction was based on the maximum gradient method, also known as the D_8 algorithm (e.g., O'Callaghan and Mark [33]). Mantilla and Gupta [25] compared the network extracted from CUENCAS with those extracted from popular GIS software such as ArcInfo, GRASS and RiverTools and found no major differences when high resolution DEMs were used. They showed that a 30m resolution DEM is sufficient to extract the drainage network that is close to the terrain's actual network. We use the one arc-second resolution (~30m) digital elevation model (DEM) from USGS to extract the channel network. This results in some 20,000 hillslopes and, thus, channel links for this basin. In Figure 1, we show the extracted channel network with links of Horton orders 4 to 7.

Section 2 indicated that the width function maxima play an important role in understanding the scaling structure of the peak flows. Figures 2(a) and 2(c) show the Horton plots for drainage areas and width function maxima of links of various orders for the Whitewater River basin, Kansas. If the channel network is self-similar, the averages of drainage areas and width function maxima display linearity with respect to the corresponding Horton orders in the log-linear domain (e.g., Strahler [45]; Peckham and

Gupta [36]; Furey and Troutman [10]). The log-linearity in Figures 2(a) and 2(c) confirm the statistical self-similarity of the upstream areas and the width function maxima. In the regression analysis, we use the areas and width function maxima corresponding to the Horton orders 2 to 6. The order 7 stream is not used in the Horton regression due to sampling reasons: we have only one point corresponding to the order 7. Although, averages corresponding to order 1 streams do not suffer from sampling issues, they are usually not considered in the regression (e.g., Peckham and Gupta [36]; Mantilla and Gupta [25]) as they represent the finest detail in a stream network, and therefore the corresponding basins do not contain a "network". The Horton ratios for the areas and width function maxima are then obtained by exponentiation of the slopes from the regression analysis. The scaling exponent of width function maxima obtained through Horton ratios in (1) is 0.49.

If the upstream areas and width function maxima display log-linearity, as shown in Figures 2(a) and 2(c), then $E[X_\omega] = E[X_1]\cdot(R_X)^{\omega-1}$, where X is either the upstream area or the width function maxima and R_X is the corresponding Horton ratio. The rescaled upstream areas and width function maxima are obtained by dividing each value of X_ω by $E[X_1]\cdot(R_X)^{\omega-1}$. The probability distribution of the quantity $X_\omega/[E[X_1]\cdot(R_X)^{\omega-1}]$ is called the rescaled probability distribution. In Figures 2(b) and 2(d), we show the statistical self-similarity of areas and width function maxima in terms of their rescaled probability distributions for orders 1 to 5. Although order 1 basins were not considered in the regression analysis, it can be seen that their rescaled probability distribution collapses onto those of orders 2 to 5.

3.2. Hydrologic Model

Because of the fundamental effect of the river network structure on peak flows, it is necessary to have a distributed hydrologic model that can calculate hydrographs for all river network links in order to carry out a systematic investigation. In this study, we used the CUENCAS model, developed by Mantilla and Gupta [25], which is based on hillslope-link decomposition of the landscape and mass conservation equations (e.g., Gupta and Waymire [16]). The model can be run with linear routing with constant flow velocity throughout the channel network or nonlinear routing with velocity that depends on the discharge in each link and the corresponding upstream area. For the nonlinear case, the velocities are estimated using (Mantilla [24])

$$V_c(t) = v_R \cdot \left(\frac{q(t)}{Q_R} \right)^{\lambda_1} \cdot \left(\frac{A}{A_R} \right)^{\lambda_2} \qquad (3)$$

where $V_c(t)$ is the velocity in the channel and A is the upstream area of the corresponding channel. The coefficients λ_1 and λ_2 are the velocity scaling exponents for discharge and upstream area, respectively, and v_R, Q_R and A_R, are reference velocity, discharge and area, whose values are taken in this study to be 1.0 m/s, 200 m^3/s and 1100 km^2. These values are obtained from measurements during the rainfall-runoff events in the Whitewater River basin. The above equation gives the instantaneous velocity as a function of discharge $q(t)$ in the channel link, which in turn gives rise to a non-linear ordinary differential equation that represents fluxes coming out of the channel link. Please see equations (6) and (9) – (11) in Mantilla et al. [26] for more details.

Although the nonlinear routing mechanism is closer to reality, we also included the linear routing analysis in this study as it is a good starting point to investigate the effect of rainfall variability on the peak flow scaling structure. Throughout this study, we use a value of 0.5 m/s for the V_c for the linear routing scenario and λ_1 and λ_2 of 0.3 and -0.1 for the nonlinear routing scenario, obtained based on field data from the region. In Figure 3, we show the velocity obtained using (3) for the link that corresponds to the largest upstream area of each Horton order for the Whitewater River basin. Throughout the study, we employed a rainfall grid of size 40×40 km^2 with a spatial resolution of 1 km. The temporal resolution and the duration of the event (simulated as well as radar data) are different for different events, as mentioned in the corresponding sections.

3.3. Assumptions

In all of our simulation scenarios, we assume (1) negligible evaporation; (2) purely surface runoff (i.e. no infiltration and no subsurface runoff); and (3) instantaneous flow of runoff into the channel. Evaporation rate is often an order of magnitude lower than storm rainfall rate, and Hortonian runoff generation is one of the main flood producing mechanisms. From the brief review of literature presented in Section 2, one can infer that the complexity in the simulation-based studies that were carried out to understand the scaling behavior of peak flows have steadily increased since the early nineties. For instance, one of the first studies was based on the deterministic Peano network and uniform rainfall (e.g., Gupta et al. [18]). Some recent studies have used random self-similar networks to mimic the river network behavior (e.g., Veitzer and Gupta [47], Mantilla [24]). We continue on this trajectory by introducing complexity one step at a

time. Therefore, in this study, the complexity is in terms of rainfall variability and the river network structure, which is why we limited our analysis to the Hortonian runoff generation mechanism. We understand that in reality, other runoff producing mechanisms are also possible in the selected study area. The hydrologic model we used can account for the saturation excess mechanism, for instance. However, including it in the study would only add additional variability, and it is difficult to separate the role of rainfall variability and the variability introduced by the saturation excess mechanism. The third assumption regarding the instantaneous flow to the channel plays a key role in shaping the hydrologic response. For smaller basins (< ~ 10 km^2), it leads to overestimation of the peak flows as the hillslope travel times are comparable to the time spent in the channel network (e.g., D'Odorico and Rigon [7]). But the error is smoothed out for larger basins.

Therefore, the assumptions are reasonable in the context of exploring the roles of rainfall and channel network on the scaling exponents of peak flows, i.e., floods, for individual rainfall-runoff events. Relaxing these assumptions and including other details such as saturation excess flood production, hillslope travel times and channel hydraulic geometry will be part of our future communications.

4. Hydrographs vs. a Scaling-based Framework

This section illustrates via simple simulation experiments the advantages of the scaling-based analysis of hydrologic response. The hydrologic model CUENCAS is forced with two simple rainfall scenarios of changing intensity (60 mm/h and 10 minutes) and duration (5 mm/h and 120 minutes), while keeping the total rainfall volume constant

(1.1×10^7 m^3). The simulated rainfall is spatially uniform over the basin for the given duration. We also assumed that the runoff is Hortonian and reaches the channel instantaneously. The discharges are normalized with respect to the peak flow corresponding to the rainfall scenario of 60 mm/h for 10 minutes. The time of occurrence is then normalized with the time at which the normalized discharge corresponding to the scenario of 60 mm/h and 10 minutes reaches 0.01. In Figure 4, we show the normalized hydrographs at six different locations in the Whitewater River basin. Although we show the normalized hydrographs at only six locations, we simulated hydrographs for all the interior sub-basins as well as for the outlet of the Whitewater River basin (Figure 1) by solving the mass and momentum equations throughout the river network. Figure 4 demonstrates that at smaller scales, the values of flow peaks differ greatly from each other and occur at different instances. However, the flow hydrographs are indistinguishable as we move to the larger scales.

We then relax the spatial uniformity assumption and assume that the rainfall is randomly distributed in space over the hillslopes of that same basin. We obtained ten realizations of the rainfall following a uniform distribution over the range of 20 to 100 mm/h with the average intensity equal to 60 mm/h and the duration kept at 10 min. That is, for each rainfall field of size 40×40 km^2, we generated 1600 random numbers following a uniform distribution with a range of [20,100] and a mean of 60 mm/h. It should be noted that these fields do not possess any spatial correlation. In Figure 5, we compare the normalized hydrographs obtained with these ten rainfall fields with the one obtained for the spatially uniform case of Figure 4. It is clear from Figure 5 that for spatially random rainfall, the variability in the hydrographs at smaller scales is higher

compared to those of larger scales. Therefore, to develop a comprehensive understanding of river basin response, it is imperative that we study the hydrographs throughout the basin across multiple scales.

In this context, the results from spatially uniform rainfall (Figure 4) can be alternatively represented in the form of Figures 6(a) and 6(b). Similarly, the results from spatially variable rainfall (Figure 5) for two of the simulated realizations are shown in Figures 6(c) and 6(d). This framework allows us to study the basin response across multiple scales. Figure 6 illustrates that our simulated peak flows display scaling structure with respect to the drainage area, and the scaling regime depends on the intensity, duration and variability of the rainfall. Figure 6 also demonstrates that the effect of rainfall variability on the basin response is scale-dependent. While peak flows are sensitive to the intensity, duration and spatial distribution of rainfall at small scales (~10 km^2), the variability in rainfall is dampened at larger scales (~1000 km^2) by the river network via aggregation of flows.

5. Basin response to the radar-rainfall data

To investigate the statistical structure of peak flows for a range of scales, it is necessary to have information on the spatial-temporal distribution of rainfall events. Such information can be conveniently provided by the ground-based weather radar network. We obtained radar estimates of three rainfall events that occurred in 2007 over Whitewater River basin, Kansas. The spatial resolution of the data is 1 km, and the temporal resolution is 15 minutes. We forced the hydrologic model CUENCAS with radar-rainfall estimates and obtained the hydrographs for all the interior sub-basins and

the outlet of the Whitewater River basin. We assumed a linear routing mechanism with constant flow velocity throughout the river network. Figure 7 shows the peak flow structure for the 6th of May 2007 event that lasted for approximately 25 hours. Figure 7 reveals that peak flows display scaling with a scaling exponent of 0.70. We obtained ordinary least squares fit to the peak flows, though in the Hortonian regression framework, similar to the width function analysis presented in the previous section. That is, instead of obtaining the scaling exponent by regression of peak flows with upstream areas, we used (2) to obtain the scaling exponent.

The scaling exponent of 0.70 is larger than the scaling exponent of the width function maxima. For the other two 2007 events that we analyzed, the scaling exponents were 0.68 and 0.77. From the studies discussed in Section 2, we know that when a spatially uniform rainfall is applied instantaneously, the peak flow scaling exponent is very close to that of the width function maxima. A real rainfall event is far from being spatially uniform and lasts for a certain duration. Therefore, the scaling exponent is different from that of the width function maxima. Figure 7 shows that the scatter at small scales is different from that of the spatially uniform or spatially random case presented in Figure 3. Another conspicuous feature in Figure 7 is that the scale break is poorly defined, possibly because of the inherent space-time variability of the rainfall event such as zero-rain intermittency and its spatio-temporal correlation structure.

The studies discussed in Section 2, which were carried out under idealized conditions, cannot clearly explain the effect of various characteristics of rainfall that resulted in Figure 7. It is also well known that remotely sensed rainfall products suffer from large uncertainties (e.g., Krajewski and Smith [21], Ciach et al. [6]) that propagate through the

hydrologic models and contribute to the variability of the predicted peak flows across scales. Consequently, it becomes necessary to separate the effects of uncertainties from the effects of variability of rainfall on the peak flow scaling structure. The natural variability of rainfall itself has a great impact on the statistical structure of peak flows, and understanding its role is the main goal of this study. Hereafter, we avoid using rainfall data and follow a systematic simulation framework to explore the effect of rainfall variability on the peak flows.

6. Simulation Scenarios and Results

We start our experiments with simple but less realistic models of rainfall and proceed to complex space-time models that yield more plausible rainfall. We obtain parameters of these models from analyzing real rainfall events.

6.1. Sensitivity to the Intensity and Duration of Spatially Uniform Rainfall

We start with the simple scenario of a basin receiving spatially uniform rainfall of a certain intensity and duration. Figure 8 shows the peak flows versus drainage areas for different rainfall intensities and durations with a linear channel routing mechanism. Three important features of the peak flow scaling structure that are apparent in the plots are the scatter, the scale break and the scaling exponent. For a fixed rainfall intensity, the scatter decreases as the duration of the event increases. For each link, there is an upper limit for the peak flow that is not exceeded. This upper limit corresponds to the equilibrium discharge reached when the rainfall duration is larger than the concentration time. With an increase in the duration of rainfall, more hillslopes reach saturation,

thereby decreasing the scatter. The peak flows for the links that reached steady-state correspond to the well known rational method $Q = c\ I\ A$, where c is the runoff coefficient, I is the rainfall intensity and A is the upstream drainage area. In this study, since the infiltration is assumed to be zero, the value of c is equal to 1.0. We obtain the scale break by comparing the peak flows obtained from our simulations to those from the above rational method equation. A window of fixed size in the logarithmic domain is moved along the upstream area axis of each panel in Figure 8. Within such a window, we compute the following ratio

$$\chi = \frac{\sum_{i=1}^{n_p} I_{p,i}}{n_p} \tag{3}$$

where $I_{p,i} = 1 \text{ if } 0.9Q_{rat} \le Q_{p,i} \le Q_{rat}$, $Q_{p,i}$ is the peak flow for the link i, Q_{rat} is the corresponding peak flow obtained from the rational method and n_p is the total number of links in the network. If the ratio χ is less than 0.75, the scale break is considered to be at the average of the upstream areas within that window. We realize that this definition of scale break is subjective. However, it serves the purpose of a qualitative comparison only. The scale break is indicated by a red line in Figure 8. As the duration of the rainfall increases, more links reach saturation and the scale break moves towards the larger areas. Because of the large scatter, we do not estimate the scale break for the shortest duration of 5 minutes.

Figure 8 shows that for a fixed duration, the scale break and scatter in the peak flow scaling structure remain unchanged with intensity. As in Section 5, we fit these peak flows in the Hortonian framework using (2). In Figure 9, we show the Horton plots of peak flows for all of the intensities and durations. The Horton ratio of peak flows is estimated considering only the orders that lie on the higher side of the scale break. Since the scale break is not obvious in the Horton plots, we select the orders for regression based on Figure 8. The Horton ratio of peak flows obtained by exponentiation of the regression slope is shown in each panel of Figure 9. The Horton ratio of peak flows and the upstream area are plugged into equation 2 to obtain the scaling exponent of the peak flows. The coefficient of the power law is obtained so that the regression line passes through the average of the peak flows corresponding to the top three orders (Figure 8). The regression equations in Figure 8 allow us to conclude that, for a fixed duration, the peak flows are linearly related to the rainfall intensities when the routing mechanism in the channels is linear. This result is similar to the one observed by Furey and Gupta [8] over the Goodwin Creek Watershed. For a fixed intensity, the scaling exponents range from 0.50 to 0.56 as the duration changes from 5 to 360 minutes. We have also noticed that the peak flow at the outlet of the basin changes linearly with the duration. The scaling exponents for all of the cases are larger than the width function scaling exponent of 0.49, which confirms the result of Mantilla et al. [26] for the Walnut Gulch watershed.

Figure 10 shows the effect of the intensity and duration of spatially uniform rainfall when the channel routing mechanism is nonlinear. The parameters selected in this study for the nonlinear routing mechanism result in different velocities in different links, and a straightforward panel to panel comparison between Figures 8 and 10 is therefore not

meaningful. We do not obtain the scale break for the shortest duration simulations for the same reason mentioned in the linear routing case. Regression is not performed for the longest duration of 360 minutes, as most of the links have reached saturation and the scale break is poorly defined. For the 120 minute duration, the fitted regression equations reveal that the scaling exponent decreases as the rainfall intensity decreases. It is also clear from Figure 10 that the relationship between flow peaks and rainfall intensities is nonlinear. The peak flow scaling exponents for all the cases of nonlinear routing are larger than the exponent of the width function maxima. They range from 0.55 for the shortest duration of 5 minutes to 0.66 when the rainfall intensity is 50 mm/h and the duration is 120 minutes. For the longest duration of 360 minutes, the scaling exponent is close to 1.0.

6.2. Sensitivity to the Advection Velocity

A spatially uniform rainfall of intensity 30 mm/h and covering approximately half the size of the basin (40×20 km^2) is moved from west to east at five different velocities (4, 8, 16, 32 and 64 km/h). It should be noted that the spatial uniformity is only within the 40×20 km^2 area; the rainfall actually received by the basin cannot be considered as uniform. The peak flows are fitted in the Hortonian framework, and the regression equations are obtained. Figure 11 plots the scaling exponents versus advection velocities for linear and nonlinear routing mechanisms. As expected from the results shown in Figure 10, there is no scale break for the smallest advection velocity of 4 km/h for the nonlinear routing mechanism, and therefore we did not perform any regression analysis. For both channel routing mechanisms, the scaling exponent decreases with an increase in

advection velocity. Our motive for plotting linear and nonlinear routing mechanisms in the same figure is not to compare them point-to-point but to compare how the exponents decrease with advection velocity. Figure 11 also shows the power law fit for both routing mechanisms. The fitted equations reveal that the trend is the same for both routing mechanisms. The decreasing trend can be explained in terms of the effect of duration discussed in the previous subsection. With the increase in advection velocity, the duration for which the block of rainfall stays over the basin decreases, and therefore the scaling exponent also decreases.

6.3. Sensitivity to the Spatial Variability of Rainfall

We have thus far assumed that the rainfall is spatially uniform throughout the basin. In this subsection, we investigate the effect of spatial variability on the scaling exponents of peak flows. Though there are many ways in which spatial variability can be characterized, we explore it in terms of variance, correlation structure and zero-rainfall intermittency. Our experiments are designed so that we depart from the uniform rainfall scenarios in a gradual, simple manner to keep from losing the benefits of the recently gained understanding of the effects of the uniform intensity and duration.

6.3.1 Simple Block Structure

We relax the spatial uniformity of rainfall over the basin by breaking it into two components: a block of uniform rainfall with an intensity of 25 mm/h for a duration of 30 minutes on the western half of the basin and a rainfall of 50 mm/h for a duration of 120 minutes over the eastern half of the basin. The channel network routing is assumed to be linear with a velocity of 0.5 m/s throughout the network. Figure 12 shows the scaling

structure of peak flows for this scenario. The banded structure apparent in Figure 12 is a direct manifestation of the different rainfall intensities received by the western and eastern regions of the basin. The scale break for these two bands also occurs at different locations because of the different rainfall durations over the western and eastern parts of the basin. We noticed a similar trend for the nonlinear routing in channels.

6.3.2 Gaussian Uncorrelated Field

In this scenario, we simulate Gaussian random fields with a mean of 25.0 mm/h and the standard deviation ranging from 0.1 mm/h to 6 mm/h. By gradually varying the variance, we gently depart from the well-understood case of uniform intensity. The duration of the rainfall is fixed at 120 minutes. The peak flow scaling structure for four different cases of standard deviation and linear routing mechanism is shown in Figure 13. In the Hortonian regression, we used the orders 3 to 7. Table 1 lists the average rainfall, intercept, scaling exponent and the peak flow at the outlet of the basin for all the cases and for both routing mechanisms. Figure 13 and Table 1 reveal that the increasing variance has no significant effect on the fitted regression equations. The main effect of the variance is to increase the scatter in the peak flow scaling structure. The scatter is averaged out by the basin at the larger scales, as seen from the peak flow values at the outlet (Table 1). The slight variation in the intercepts and outlet peak flows is expected given that we are using realizations of a random process. This is further evident from the estimated values of the mean, which are different from the theoretical value of 25 mm/h.

6.3.3 Gaussian Correlated Field

To investigate the effect of the spatial correlation of the rainfall field on the scaling exponents, we obtain Gaussian fields with a mean of 25 mm/h and a standard deviation of 2 mm/h and that is characterized by an exponential correlation structure

$$\rho(d) = \theta_0 \cdot \exp\left[-\left(\frac{d}{\theta_1} \right)^{\theta_2} \right] \quad (4)$$

where θ_0 characterizes the nugget effect and the small scale variability, θ_1 is the correlation distance defined as the distance at which the correlation drops to 1/e and θ_2 is the shape factor that controls the shape of the correlation function at the origin. We fixed the nugget parameter and the shape factor at one and generated the random fields with the correlation distances varying from 5 km to 50 km. Each field is then applied for 120 minutes over the basin, and the peak flows are estimated for linear and nonlinear routing mechanisms. Figure 14 shows the scaling structure of peak flows for two extreme cases of correlation distances and a linear routing mechanism. The effect of increasing correlation is to decrease the scatter in the scaling structure (Figure 14). Table 2 shows that the larger scale basin response is almost independent of the correlation structure, although there is some variability in the intercepts and outlet peak flows, which is mainly due to the fact that we are using realizations of a random process.

6.3.4 Spatial Zero-Rain Intermittency: Uncorrelated Random Fields

To investigate the effect of zero-rainfall intermittency, we simulated random rainfall with varying degrees of zero-rainfall intermittency and a duration of 120 minutes. The value of rainfall over each pixel was drawn from uniform distribution U[10,30], and intermittency is introduced randomly but maintains an overall mean fixed at 20 mm/h. We considered four values of intermittencies: 0.0, 0.05, 0.25 and 0.50 (corresponding rainy area fractions are 1.0, 0.95, 0.75 and 0.50). These rainfall scenarios were supplied as input to the CUENCAS model, and the peak flow scaling structure was obtained for linear routing mechanisms. The sensitivity of the peak flow scaling to the intermittent random fields is shown in Figure 15. With the increase in intermittency (or decrease in rainy area), the scatter for the smaller scale basin peak flows increased. However, the effect of intermittency is reduced for the larger scale basins, as evidenced by the linear regression equations shown in each panel of Figure 15 and also from the outlet peak flow values shown in Table 3. The simulations are repeated for the nonlinear routing mechanism, and we found a similar pattern to the pattern found in linear routing, although the intercepts and scaling exponents differed (Table 3).

6.3.5 Spatial Zero-Rain Intermittency: Correlated Random fields

To study the effect of intermittency in a more realistic manner, we selected the spatial component of the rainfall model developed by Bell [2]. The model belongs to the class of meta-Gaussian models (e.g., Mejia and Rodriguez-Iturbe [27]; Bell [2]; Guillot and Lebel [13]) and generates a two-dimensional isotropic, correlated random field using spectral analysis. A non-linear transformation and an external threshold are then applied

to obtain a rainfall field with desired intermittency, average intensity and correlation structure. In Bell [2], the use of exponential transformation resulted in lognormally distributed rainfall. The parameters for the model are the log-transformed (Gaussian) mean and variance of the rainy area, the zero-rainfall intermittency factor and the spatial correlation structure. The parameters we selected are 0 and 0.5 for the log-transformed mean and variance of the rainy area and exponential correlation structure with a correlation distance of 20 km. We observed that the realizations from the model, besides having the desired spatial correlation structure, also displayed spatial scaling behavior (not shown). The duration of the event is fixed at 120 minutes. To keep the volume constant with changing intermittency, we simulated a single realization with a given correlation structure on a large (256×256) domain and selected the portion that yielded the desired intermittency and volume. The spatial structure of the field thus obtained will remain the same as the larger one. Figure 16 shows the scaling structure of peak flows for four different intermittency factors starting from 0 to 0.50 for the linear channel routing mechanism. Unlike in Figure 15, significant scatter was observed even for higher order basins (particularly for the bottom panels of Figure 16) when the pixels are correlated. The large scatter is due to the high probability of concentrated intermittent pixels present in correlated intermittent fields. Whereas, for uncorrelated intermittent fields, the river network efficiently aggregates the randomness in the fields. However, the overall behavior - of increasing scatter with increasing intermittency - is similar for both scenarios.

7. Simulations from the Space-time Rainfall Model

The scenarios investigated so far have offered insight into the effects of different characteristics of rainfall on the spatial scaling structure of peak flows. We will now investigate the basin's response to more realistic space-time rainfall events. Therefore, we have simulated a space-time rainfall event from a model developed by Bell [2] and applied it over the basin. The spatial component of the model is described in the previous section. The temporal evolution of the rainfall is modeled as an autoregressive process with parameters based on the correlation time of area-averaged rainfall. The parameters for the model are obtained by analyzing several storms over the Midwest. In this study, we simulate two different storm events with characteristics listed in Table 3. Storm 2 is more variable than storm 1, as seen from the values of the coefficient of variation and correlation distance. Another important difference is that storm 1 lasts longer and has larger values of mean and rainy fraction compared to storm 2. The values of the shape factor suggest that storm 2 is more correlated at very small scales than storm 1.

Figure 17 shows the basin response to the two storms for the linear routing mechanism. The peak flow scaling structure for this complex scenario can now be explained using the results from Section 6. Figure 17 considers three components: scale break, scatter and regression equations. Although the scale break is sharp and evident for the simulation scenarios of Section 6 under idealized conditions, it is not clearly seen in the peak flow scaling structure resulting from the simulated realistic space-time rainfall event. Since the scaling exponent is not close to 1.0, basin saturation (for instance, top panels of Figure 8) is not the reason for the absence of scale break. The lack of sharp

scale break for realistic rainfall scenarios can be best explained by revisiting the idealized scenarios in Section 6. For instance, a combination of just two different intensities and durations has diffused the scale break in Figure 12. The space-time rainfall fields are characterized by different intensities, durations, correlations and intermittencies and move with a certain advection velocity. In a way, these fields are a combination of all of the scenarios considered in Section 6. This explains the absence of scale break for storm 1.

The scatter for storm 1 is smaller than that of storm 2. Two main factors responsible for the reduced scatter are the duration of the storm and zero-rain intermittency. Results from Section 6.1 indicate that one consequence of longer duration events is the decreased scatter that is most pronounced at smaller scales. In Section 6.3.4 that pertains to the effect of zero-rain intermittency, we note that the scatter in the peak flow structure increases rapidly as the area of rainfall decreases. Though the rainy fraction of storm 1 is 46 %, the advection of the storm eventually increases the effective wetted area of the basin, thereby decreasing the scatter seen at smaller scales. For the second storm, the large scatter is due to the increased intermittency combined with the shorter duration and large coefficient of variation.

The regression equation seen for storm 1 is obtained in a Hortonian framework using the orders 2 to 7. For storm 2, peak flows corresponding to the Horton orders of 4 to 7 are used in this storm's regression. The scaling exponent for both storms is larger than the scaling exponent of the width function maxima. For the nonlinear routing scenario (not shown), we noticed a similar pattern with larger scatter and higher values for scaling exponents than in the linear routing case.

8. Analysis of Scatter

The scatter in the peak flow scaling structure for the lower order basins can be explained in terms of peak flows reaching equilibrium (basins reaching saturation), while the scatter for the higher order basins can be explained in terms of aggregation and attenuation of flows. We illustrate this by analyzing the peak flows for two of the rainfall scenarios in Section 6.1 and Figure 8. Specifically, we compare the probability distributions of the rescaled peak flows corresponding to spatially uniform rainfall of 5 mm/h and durations of 5 and 120 minutes with the probability distributions of rescaled areas and width function maxima. Figure 18(a) illustrates that for a spatially uniform rainfall intensity of 5 mm/h and a duration of 120 minutes, the order 1 probability distributions of rescaled peak flows and areas are indistinguishable (negligible scatter in Figure 8), but for a shorter duration of 5 minutes, the probability distributions are very different (large scatter in Figure 8). Since the width function maxima have the signature of the aggregation of flows in the channel network, we compare the order 5 probability distributions of rescaled peak flows and width function maxima in Figure 18(b). We intended to compare the probability distribution of peak flows with that of width function maxima for higher order basins. However, for orders 6 and 7, there are not enough points to obtain the probability distributions. Therefore, we limit the comparison to order 5 basins. Unlike the order 1 distribution, the order 5 distribution is not very sensitive to the duration of the rainfall event. For both rainfall scenarios, the distributions of rescaled peak flows match reasonably well with those of width function maxima (Figure 18b).

9. Remarks

While our results are subject to the usual limitations of a simulation study, our experiments contain many realistic aspects. First, our river basin has a substantially larger size (scale) than many small experimental basins that are the basis for many hydrologic studies. Second, using high-resolution DEM data, we extracted a river network that closely approximates the actual drainage pattern of the selected basin. Third, our rainfall variability cases and range of values, though simple, capture the key aspects of natural rain systems.

We modeled rainfall space-time variability in terms of stationary random fields with a certain intermittency and correlation structure in space and time. Although the emphasis of this approach is more on generation of space-time random fields and lacks a direct link to the physical aspects of the rainfall process, one can qualitatively relate the statistical parameters to the meteorological aspects such as back-building thunderstorms, squall lines and convective systems. For instance, the size of the convective system with respect to the size of the basin is an important characteristic that controls the basin response. This information is embedded in the correlation distance and shape factor in equation 4. There are other ways of characterizing the space-time variability of rainfall fields such as modeling of rainfall based on spatial cluster processes for rain cells, dynamic modeling of rainfall based on partial differential equations for mass and momentum conservation and scaling-based modeling of rainfall space-time structure. It would be interesting to employ these models and relate the parameters of rainfall models to the characteristics of peak flow scaling structure.

Anthropogenic alteration of the landscape will have an impact on the extracted drainage network and subsequently on the aggregation of the flows affecting the larger scale basin response. The hydraulic geometry of the channels is another key factor which is strongly related to the channel-floodplain interactions and influences the storage zones, movement of the flood waves and the travel time within the channel. Therefore, it is expected to have an influence on the peak flow scaling structure. The CUENCAS framework allows for the inclusion of this feature by modifying the local velocity law. However, investigation of this factor is beyond the scope of this work, and our strategy is to avoid any aspects in the dynamics that can obscure the effect of rainfall variability.

Throughout this study, we have estimated the Horton ratios by ordinary least squares regression of logarithms of arithmetic averages with the Horton order (See Figure 2). Based on a simulation study, Furey and Troutman [10] suggested the use of individual quantities (for example, areas or peak flows) instead of arithmetic averages. Since the main focus of the study is on the role that rainfall variability plays in the scaling structure of peak flows, our use of arithmetic averages instead of individual quantities in the Horton analysis would not affect the results. Also, in this study, we have assumed that the runoff generation is Hortonian with no infiltration so that we can focus on the role that rainfall plays in the statistical structure of peak flows. The key issue is how to specify the infiltration threshold for each of 20,000 hillslopes in CUENCAS, which differ due to spatial variability in soil and vegetation properties. This problem of “dynamic parametric complexity” is a major research problem (e.g., Gupta [14] and Furey and Gupta [9]) and not addressed in this study.

10. Summary and Conclusions

In this study, we carried out a systematic investigation to understand the role that rainfall plays in the spatial structure of peak flows. Due to the lack of adequate field data, i.e., numerous stream gauges as well as highly accurate rainfall maps, we used simulations. Our simulation experiments consisted of simple scenarios aimed at isolating the effects of rainfall variability on the peak flow scaling structure. We demonstrated that rainfall variability has a different impact on the magnitude of peak flows for basins of different scales. We selected the Whitewater River basin in Kansas for this study and a distributed hillslope-link based hydrological model to obtain the peak flows for each link within the basin. The channel network that was extracted is characterized in terms of width function maxima. The width function maxima of the Whitewater River basin displayed scaling behavior with respect to the Horton orders. The scaling exponent of width function maxima was estimated to be 0.49.

We focused on three aspects of the peak flow scaling structure for all the scenarios: scatter, scale break and the scaling exponents. The results showed that the peak flow scaling exponents for all the scenarios considered in this study are greater than the width function scaling exponent. This result is in agreement with the hypothesis of Mantilla et al. [26] that in the river networks, the peak flow scaling exponent is governed by the competition between the attenuation and aggregation of the flows. For a fixed intensity, the scaling exponent increases with an increase in the rainfall duration, and for a fixed duration, the scaling exponent does not change with intensity for linear channel routing and decreases with intensity for nonlinear channel routing. For the two hour duration, the

fitted regression equations reveal that the scaling exponent decreases as the rainfall intensity decreases. Based on simulations with spatially uniform rainfall of varying depths and a fixed duration of 10 minutes on a deterministic Mandelbrot-Viscek network, Menabde and Sivapalan [28] reported that the scaling exponent increases as the rainfall depth decreases. For the Whitewater River basin, and therefore in a real river network, we did not notice such a trend for 30 and 5 minute duration simulations and noticed a reverse trend when the duration was 120 minutes.

For a constant volume of rainfall, the effect of spatial variability, as characterized by variance, spatial correlation and the spatial intermittency, is to increase the scatter in the peak flow scaling structure. At larger scales, the effect of variability decreases, as seen from the regression equations and peak discharges at the outlet of the basin (Tables 1, 2 and 3). Based on the simulations on a deterministic Mandelbrot-Viscek network, Menabde and Sivapalan [28] reported that the variability in the rainfall decreases the scaling exponent of peak flows on both sides of the scale break. We did not observe such behavior in our simulations. For homogeneous rainfall fields and under idealized conditions of flow routing on hillslopes and in channels, we observed that the smaller scale basin response was dominated by the rainfall intensity (and spatial distribution), while the hydrologic response of larger scale basins was driven by rainfall volume, river network topology and flow dynamics. We expect that the heterogeneity in rainfall will have similar behavior, at least for the larger scale basins as the river network aggregates the heterogeneity. However, heterogeneity in rainfall will have a larger impact for smaller scale basins.

The results obtained from the above simple scenarios enhanced our understanding of the peak flow scaling structure obtained from simulated space-time variable rainfall. Storm duration and advection are the key factors that control the effective zero-rain intermittency, which in turn affects the scatter in the peak flows. The peak flow scaling structure for the realistic space-time rainfall scenarios did not present a clear and sharp scale break. The scale break was masked due to the inherent space-time variability in the realistic rainfall fields.

The results in this study also foster the development of a scaling based predictive framework for peak flows using remotely sensed rainfall products over basins ranging from very small to very large scales. A key question is, "What is the scale at which remote sensing products provide meaningful predictions?" Our results suggest that the variability contributed by random errors of remote sensing sensors, such as weather radars and satellites, are filtered out by the drainage structure of river basins at some scales. Investigations of the above problem are underway and require models of uncertainty such as those developed by Ciach et al. [6], Villarini et al. [49] and Villarini and Krajewski [48].

Acknowledgments

The authors recognize support from the National Science Foundation grant EAR-0450320, the Rose & Joseph Summers endowment to The University of Iowa and IIHR-Hydroscience & Engineering. We also acknowledge valuable discussions with Dr. Thomas Bell regarding the space-time model of rainfall.

REFERENCES

[1]. C.V. Alonso and R.L. Binger. Goodwin Creek experimental watershed: a unique field laboratory. Journal of Hydraulic Engineering 2000; 126: 174-177.

[2]. Bell, T.L. A space-time stochastic model of rainfall for satellite remote sensing studies. Journal of Geophysical Research 1987; 92: 9631-9643.

[3]. Beven, K.J. Rainfall-Runoff Modeling - The Primer, Wiley, Chichester 2001; 356 pp.

[4]. Bloschl, G., and M. Sivapalan. Process controls on regional flood frequency: Coefficient of variation and basin scale. Water Resources Research 1997; 33: 2967-2980.

[5]. Bras R.L., and I. Rodriguez-Iturbe. Random Functions and Hydrology. Dover 1993; 559 pp.

[6]. Ciach, G.J., W.F. Krajewski and G. Villarini, Product-error-driven uncertainty model for probabilistic quantitative precipitation estimation with NEXRAD data, Journal of Hydrometeorology. 2007; 8: 1325-1347.

[7]. D'Odorico, P., and R. Rigon, Hillslope and channel contributions to the hydrologic response. Water Resources Research 2003; 39: 1113, doi:10.1029/2002WR001708.

[8]. Furey, P.R., and V.K. Gupta. Effects of excess rainfall on the temporal variability of observed peak-discharge power laws. Advances in Water Resources 2005; 28: 1240-1253.

[9]. Furey, P.R., and V.K. Gupta. Diagnosing peak-discharge power laws observed in rainfall–runoff events in Goodwin Creek experimental watershed. Advances in Water Resources 2007; 30: 2387-2399.

[10]. Furey, P.R., and B.M. Troutman. A consistent framework for Horton regression statistics that leads to a modified Hack's law Geomorphology 2008; 102: 603-614.

[11]. Goodrich, D.C., Lane L.J., Shillito, R.M., and S.N. Miller. Linearity of basin response as a function of scale in a semiarid watershed. Water Resources Research 1997; 33: 2951-2965.

[12]. Goodrich, D.C., T.O. Keefer, C.L. Unkrich, M.H. Nichols, H.B. Osborn, J.J. Stone, and J.R. Smith. Long-term precipitation database, Walnut Gulch Experimental Watershed, Arizona, United States. Water Resources. Research 2008; 44: W05S04, doi:10.1029/2006WR005782.

[13]. Guillot, G., and T. Lebel. Disaggregation of Sahelian mesoscale convective system rain fields: Further developments and validation. Journal of Geophysical Research 1999; 104: 31533-31551.

[14]. Gupta, V.K. Emergence of statistical scaling in floods on channel networks from complex runoff dynamics. Chaos, Solitons and Fractals 2004; 19: 357-365.

[15]. Gupta, V.K., and D.R. Dawdy. Physical interpretation of regional variations in the scaling exponents of flood peaks. Hydrologic Processes 1995; 9: 347-361.

[16]. Gupta, V.K., and E. Waymire. Spatial variability and scale invariance in hydrologic regionalization. Scale Dependence and Scale Invariance in Hydrology, G. Sposito (Ed.), 1998; 88-135.

[17]. Gupta, V.K., Mesa, O.J., and D.R. Dawdy. Multiscaling theory of flood peaks: Regional quantile analysis. Water Resources Research 1994; 30: 3405-3421.

[18]. Gupta, V.K., Castro, S.L., and T.M. Over. On Scaling exponents of spatial peak flows from rainfall and river network geometry. Journal of Hydrology 1996; 187: 81-104.

[19]. Gupta, V.K., Troutman, T.M., and D.R. Dawdy. Towards a nonlinear geophysical theory of floods in river networks: An overview of 20 years of progress. Nonlinear Dynamics in Geosciences, Edited by Tsonis, A.A., and J. Elsner 2007; 1-31.

[20]. Horton, R.E. Erosional development of streams and their drainage basins: Hydrophysical approach to quantitative morphology, Geological Society of America Bulletin 1945; 56: 275–370.

[21]. Krajewski, W.F., and J.A. Smith, Radar hydrology: rainfall estimation. Advances in Water Resources 2002; 25: 1387–1394.

[22]. Krajewski, W.F., Lakshmi, V., Georgakakos, K.P., and S.C. Jain. A Monte Carlo study of rainfall sampling effect on a distributed catchment model. Water Resources Research 1991; 27: 119-128.

[23]. Lashermes, B., and E. Foufoula-Georgiou. Area and width functions of river networks: New results on multifractal properties. Water Resources Research 43; 2007: W09405, doi:10.1029/2006WR005329.

[24]. Mantilla, R. Physical basis of statistical self-similarity in peak flows on random self-similar networks, PhD dissertation 2007, University of Colorado, Boulder.

[25]. Mantilla, R., and V.K. Gupta. A GIS numerical framework to study the process basis of scaling statistics in river networks. IEEE Geoscience and Remote sensing letters 2005; 2: 404-408.

[26]. Mantilla, R., Gupta, V.K., and O.J. Mesa. Role of coupled flow dynamics and real network structures on Hortonian scaling of peak flows. Journal of Hydrology 2006; 322: 155-167.

[27]. Mejia, J., and I. Rodriguez-Iturbe. On the synthesis of random fields sampling from the spectrum: An application to the generation of hydrologic spatial processes. Water Resources Research 1974; 10: 705-711.

[28]. Menabde, M., and M. Sivapalan. Linking space-time variability of river runoff and rainfall fields: a dynamic approach. Advances in Water Resources 2001; 24: 1001-1014.

[29]. Menabde, M., Veitzer, S., Gupta, V., and M. Sivapalan. Tests on peak flow scaling in simulated self-similar river networks. Advances in Water Resources 2001; 24: 991-999.

[30]. Morrison, J.E., and J.A. Smith. Scaling properties of flood peaks. Extremes 2001; 4: 5-22.

[31]. Moussa, R. What controls the width function shape, and can it be used for channel network comparison and regionalization? Water Resources Research, 2008; 44: W08456, doi:10.1029/2007WR006118.

[32]. Nicotina, L., Alessi Celegon, E., Rinaldo, A., and M. Marani. On the impact of rainfall patterns on the hydrologic response. Water Resources Research 2008; 44, W12401, doi:10.1029/2007WR006654.

[33]. O'Callaghan, J.F., and D. Mark. The extraction of drainage networks from digital elevation data. Computer Vision, Graphics, Image Processing 1984; 28: 328–344.

[34]. Ogden, F.L., and D.R. Dawdy. Peak discharge scaling in small Hortonian watershed. Journal of Hydrologic Engineering 2003; 8: 64-73.

[35]. Ogden, F.L., and P.Y., Julien. Runoff sensitivity to the temporal and spatial rainfall variability at runoff plane and small basin scales. Water Resources Research 1993; 29: 2589-2597.

[36]. Peckham, S.D., and V.K. Gupta. A reformulation of Horton's laws for large river networks in terms of statistical self-similarity. Water Resources Research 1999; 35: 2763-2777.

[37]. Robinson, J.S., and M. Sivapalan. An investigation into the physical causes of scaling and heterogeneity of regional flood frequency. Water Resources Research 1997; 33 1045-1059.

[38]. Robinson, J.S., M. Sivapalan, and J.D. Snell. On the relative roles of hillslope processes, channel routing, and network geomorphology in the hydrologic response of natural catchments. Water Resources Research 1995; 31: 3089-3101.

[39]. Rodriguez-Iturbe, I., and A. Rinaldo. Fractal River Basins: Chance and Self-Organization. Cambridge University Press, New York, 1997; 542pp.

[40]. Singh V.P., and D.K. Frevert (eds). Mathematical models of small watershed hydrology. Water Resources Press, Highlands Ranch, Colorado 2002a; 972 pp.

[41]. Singh V.P., and D.K. Frevert (eds). Mathematical models of large watershed hydrology. Water Resources Press, Highlands Ranch Colorado 2002b; 972 pp.

[42]. Sivapalan, M. Takeuchi, K. Franks, S.W., Gupta, V.K., Karambiri, H., Lakshmi, V., Liang, X., McDonnell, J.J., Mendiondino, E.M., O'Connell, P.E., Oki, T., Pomeroy, J.W., Schertzer, D., Uhlenbrook, S., and E. Zehe. IAHS decade on prediction in ungauged basins (PUB), 2003-2012: Shaping an exciting future for the hydrologic sciences. Hydrologic Sciences Journal 2003; 48: 857-880.

[43]. Smith, J.A. Representation of basin scale in flood peak distribution. Water Resources Research 1992; 28: 2993-2999.

[44]. Strahler, A. N. Hypsometric (area-altitude) analysis of erosional topography. Geological Society of America Bulletin 1952; 63: 1117–1142.

[45]. Strahler, A.N. Quantitative analysis of watershed geomorphology, Transactions of American Geophysical Union 1957; 38: 913-920.

[46]. Troutman, B.M., and T.M. Over. River flow mass exponents with fractal channel networks and rainfall. Advances in Water Resources 2001; 24: 967-989.

[47]. Veitzer, S.A., and V.K. Gupta. Statistical self-similarity of width function maxima with implications to floods. Advances in Water Resources 2001; 24: 955-965.

[48]. Villarini, G. and W.F. Krajewski, Evaluation of the research-version TMPA three-hourly 0.25°×0.25° rainfall estimates over Oklahoma, Geophysical Research Letters, 34, L05402, doi:10.1029/2006GL029147, 2007.

[49]. Villarini, G., W.F. Krajewski, G.J. Ciach and D.L. Zimmerman, Product-error-driven generator of probable rainfall conditioned on WSR-88D precipitation estimates, Water Resources Research 2009; 45: W01404, doi:10.1029/2008WR006946.

List of Tables

List of Figures

Figure. 6 Scaling of peak flows with respect to the upstream areas of all the sub-basins in the Whitewater River basin. For (a) and (b), the rainfall is spatially uniform with intensity and duration indicated on the panels. For (c) and (d), the rainfall is random in space with the intensities following the uniform distribution U [20, 100] mm/h, and the duration is equal to 10 min.

Figure. 7 Scaling of peak flows with respect to the upstream areas of all the sub-basins in the Whitewater River basin, Kansas. The rainfall data is obtained from the KICT NEXRAD weather radar in Wichita, Kansas. The color scheme indicates the Horton orders as in Fig. 6.

Figure. 8 Sensitivity of peak flow scaling structure to intensity and duration of spatially uniform rainfall and linear channel routing with a velocity of 0.5 m/s. The solid black line represents the ordinary least squares fit (equation on each panel) obtained in the Hortonian framework. The color scheme indicates the Horton orders as in Fig. 6. The solid red line indicates the scale break.

Figure. 9 Horton plots of peak flows for different combinations of intensity and duration of spatially uniform rainfall applied throughout the basin. The solid line indicates the ordinary least squares regression fit. The corresponding Horton ratios are also indicated on each panel.

Figure. 10 Sensitivity of the peak flow scaling structure to intensity and duration of spatially uniform rainfall and nonlinear channel routing. The solid black line represents the ordinary least squares fit (equation on each panel) performed in the

Hortonian framework. The color scheme indicates the Horton orders as in Fig. 6. The solid red line indicates the scale break.

Figure. 11 Sensitivity of the scaling exponent of peak flows to the advection velocity of spatially uniform rainfall of intensity 30 mm/h and linear and nonlinear channel routing mechanisms.

Figure. 12 Effect of space–time variability of rainfall on the peak flow scaling structure. The rainfall is taken to be spatially uniform with the intensity of 25 mm/h for 30 min over the western half of the basin. For the eastern half of the basin, the rainfall is 50 mm/h for 120 min. The color scheme indicates the Horton orders as in Fig. 6.

Figure. 13 Sensitivity of the peak flow scaling structure to the variance of the rainfall field. The rainfall field is assumed to be Gaussian with a mean of 25 mm/h and the variance indicated on each panel. The color scheme indicates the Horton orders as in Fig. 6.

Figure. 14 Sensitivity of the peak flow scaling structure to the spatial correlation of the rainfall field. The rainfall field is assumed to be Gaussian with a mean of 25 mm/h and a standard deviation of 2.0 mm/h. The spatial structure of the rainfall field is characterized by an exponential correlation structure with the correlation distance indicated on each panel. The color scheme indicates the Horton orders as in Fig. 6.

Figure. 15 Sensitivity of the peak flow scaling structure to the zero-rainfall intermittency in rainfall fields. The rainfall fields are distributed randomly in space with the value ateach pixel drawn from uniform distribution U [10, 30] with a mean of 20 mm/h and a duration of 120 min. The color scheme indicates the Horton orders as in Fig. 6.

Figure. 16 Sensitivity of the peak flow scaling structure to the spatial intermittency of the rainfall field. The rainy portion of the field is assumed to follow lognormal distribution. We did not show the regression equations as the peak flow scaling structure is too noisy to perform Hortonian regression for the bottom two panels of the figure. The color scheme indicates the Horton orders as in Fig. 6.

Figure. 17 Response of the watershed to the simulated space–time rainfall events. The characteristics of the storms are listed in Table 3. The color scheme indicates the Horton orders as in Fig. 6.

Figure. 18 Probability distributions of rescaled areas, width function maxima and peak flows for order 1 and order 5 basins.

Table 1: Sensitivity of intercepts, scaling exponents and outlet peak flows to the variance of the Gaussian rainfall field with a mean intensity of 25 mm/h.

$N(\mu,\sigma^2)$	Mean [mm/h]	Linear Routing			Nonlinear Routing		
		Intercept	Slope	Outlet Peak Flow [m^3/s]	Intercept	Slope	Outlet Peak Flow [m^3/s]
N(25,0.1)	24.99	12.02	0.54	587.54	12.79	0.63	1246.87
N(25,1.0)	24.98	12.00	0.54	587.13	12.73	0.63	1245.98
N(25,4.0)	25.02	12.00	0.54	587.01	12.74	0.63	1246.65
N(25,9.0)	24.93	12.08	0.54	588.67	12.85	0.63	1228.01
N(25,16.0)	25.09	11.95	0.54	580.44	12.70	0.64	1249.81
N(25,25.0)	24.88	11.93	0.54	587.15	12.70	0.63	1243.16
N(25,36.0)	24.88	11.97	0.54	589.58	12.64	0.64	1252.31

Table 2: Sensitivity of intercepts and scaling exponents to the spatial correlation structure of the rainfall field. The rainfall field is assumed to be Gaussian with a mean intensity of 25 mm/h and a variance of 2.0 mm/h and is characterized by an exponential correlation function with the correlation distances indicated in the Table.

Correlation Distance [km]	Mean [mm/h]	Linear Routing			Nonlinear Routing		
		Intercept	Slope	Outlet Peak Flow [m^3/s]	Intercept	Slope	Outlet Peak Flow [m^3/s]
5.0	25.06	12.19	0.54	581.92	12.99	0.63	1232.85
10.0	24.41	11.92	0.54	566.09	12.67	0.63	1192.25
20.0	24.83	11.86	0.54	582.06	12.62	0.64	1222.65
30.0	26.49	12.54	0.54	619.69	13.44	0.64	1340.37
40.0	25.48	12.33	0.54	597.79	13.17	0.63	1279.25
50.0	23.46	11.29	0.54	545.59	11.88	0.63	1120.85

Table 3: Sensitivity of intercepts and scaling exponents to the intermittency in the uncorrelated random fields. The value of rainfall over each pixel was drawn from a Uniform distribution U[10,30], and the duration of the event is 120 minutes. The mean of the field is kept constant for different intermittencies.

Intermittency [%]	Mean [mm/h]	Linear Routing			Nonlinear Routing		
		Intercept	Slope	Outlet Peak Flow [m^3/s]	Intercept	Slope	Outlet Peak Flow [m^3/s]
0	19.88	11.45	0.50	464.66	12.26	0.58	898.48
5	20.04	11.73	0.50	473.95	12.23	0.58	907.88
25	20.05	11.23	0.50	469.37	11.58	0.58	907.24
50	19.84	11.91	0.50	485.78	12.41	0.58	942.22

Table 4: Characteristics of rainfall events simulated from the space-time rainfall model. A two parameter exponential correlation function is used to characterize the spatial dependence.

	Mean [mm/h]	Standard Deviation [mm/h]	Coefficient of Variation [mm/h]	Correlation Distance [km]	Shape Factor	Rainy Area [%]	Duration [hr]
Storm 1	3.97	10.37	2.61	15.40	0.73	45.84	20
Storm 2	1.41	5.97	4.23	5.52	0.92	17.51	4

Figures

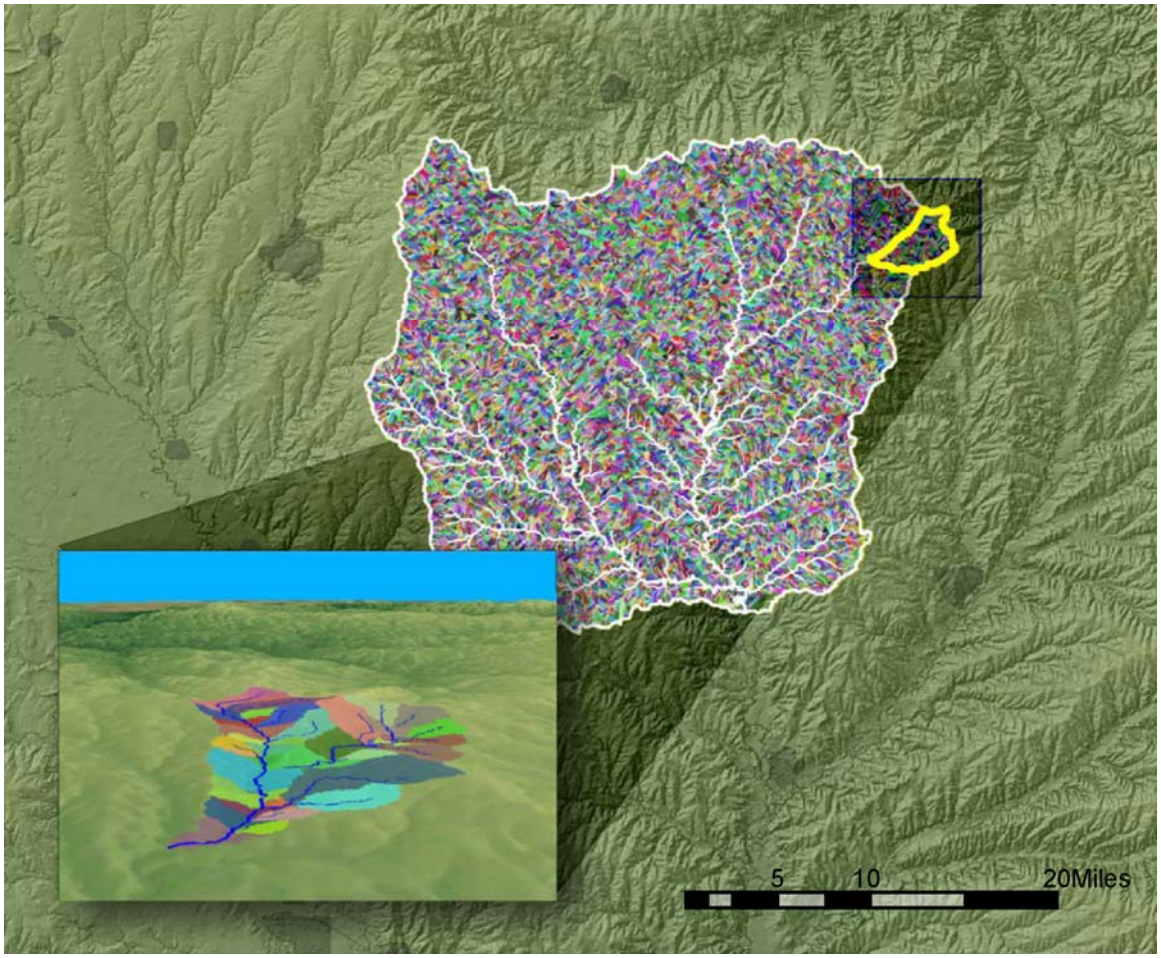

Figure 1: A shaded relief map of the Whitewater River basin showing the hillslope and channel link structure of the CUENCAS model. The channel network with links of order 4 to 7 is shown.

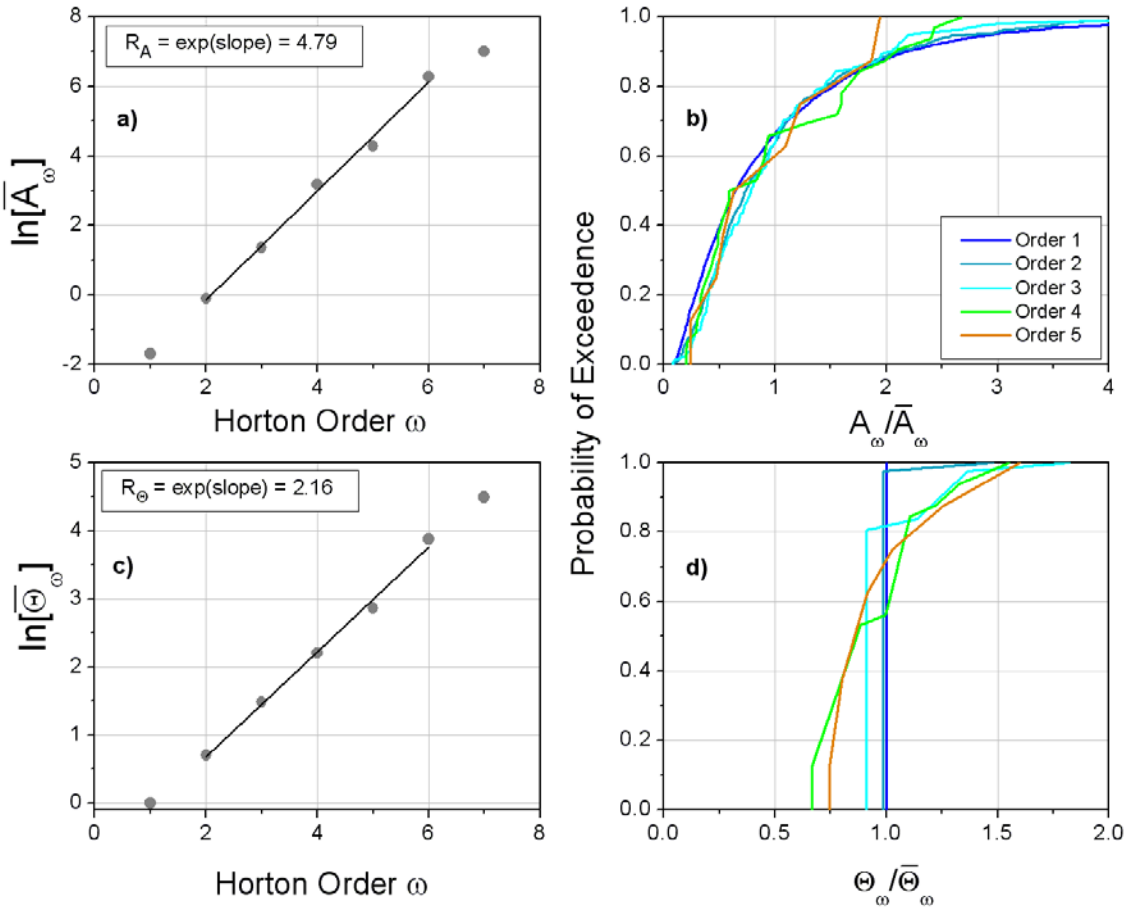

Figure 2: Statistical self-similarity of upstream areas and width function maxima in terms of Horton plots (left panels) and rescaled distributions (right panels). The ordinary least square regression is used to obtain the corresponding Horton ratios. The first order and seventh order links are not considered in fitting.

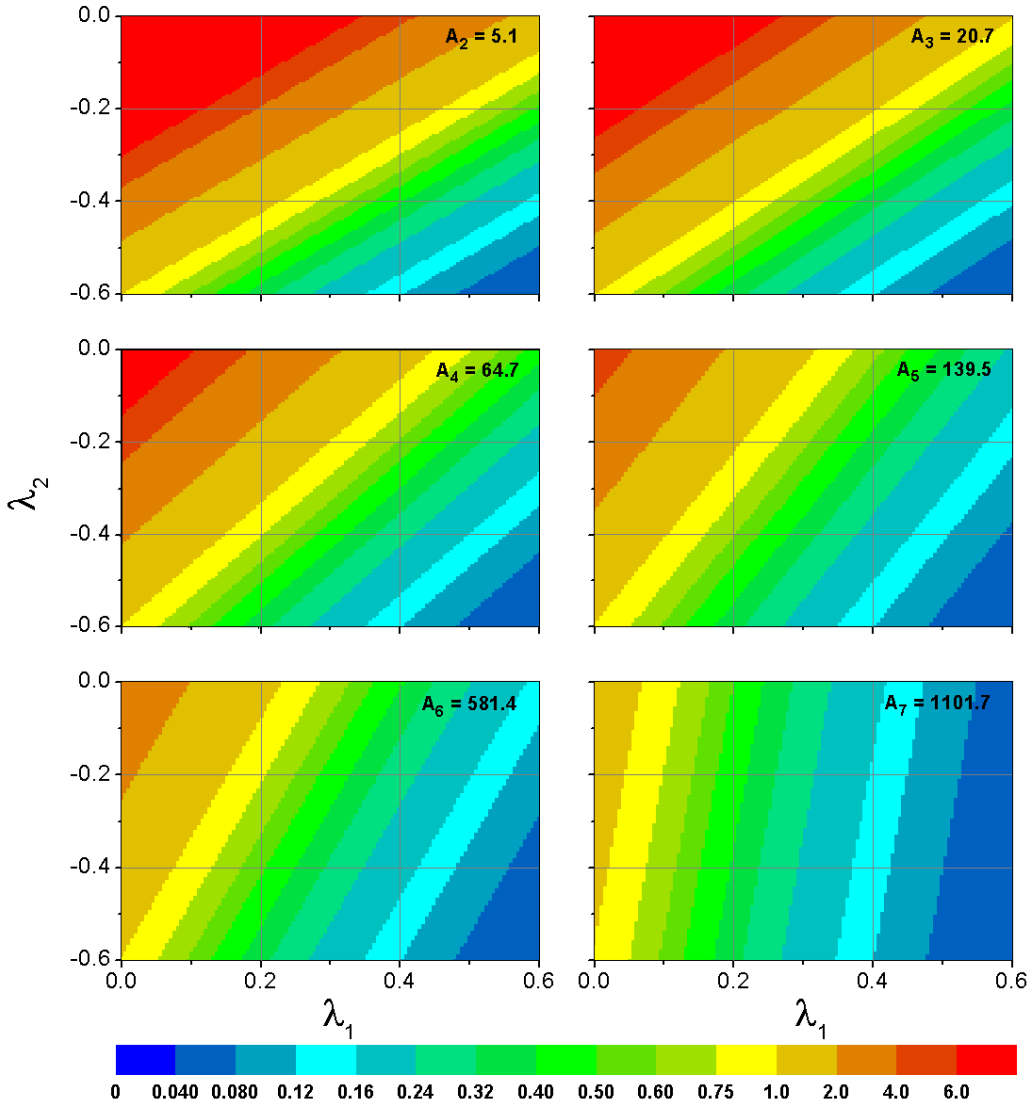

Figure 3: Sensitivity of the channel velocity (m/s) to the λ_1 and λ_2 in equation 3. The velocities are shown only for the channels that correspond to the largest area (displayed on each panel) for the Horton orders 2 to 7. The area units are in km^2.

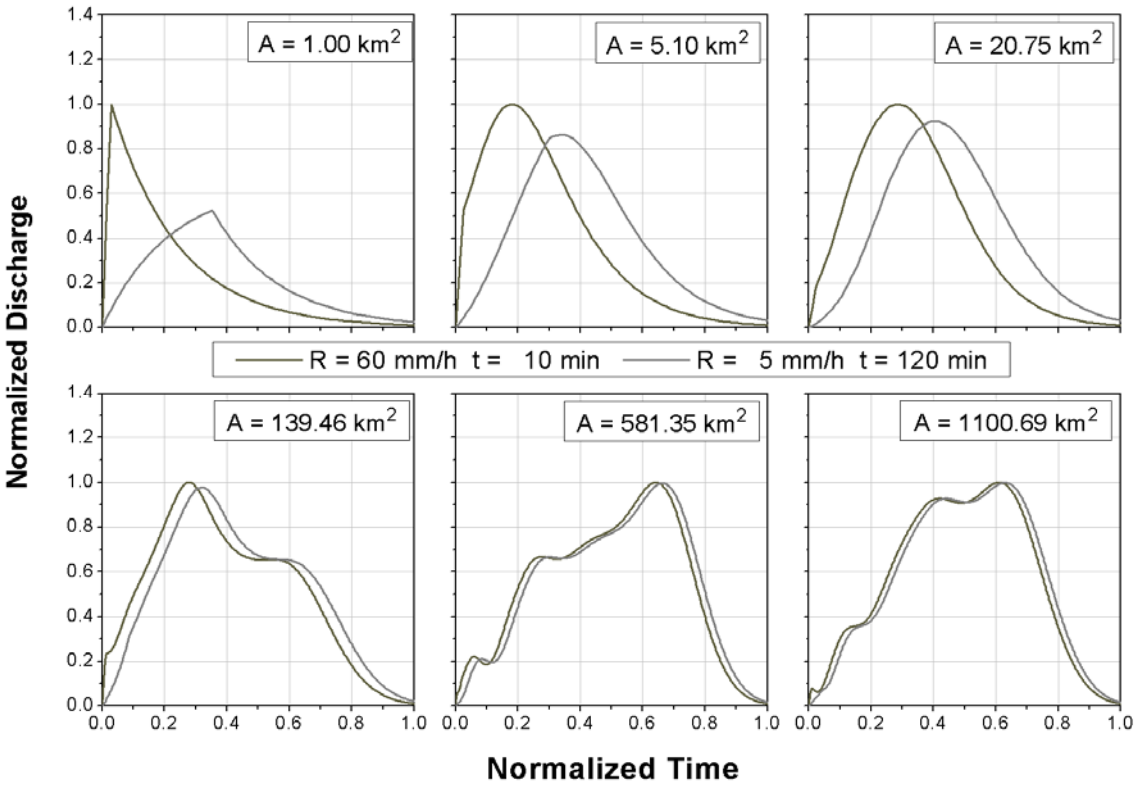

Figure 4: Hydrographs at six locations in the Whitewater River basin obtained from a distributed hydrologic model for a spatially uniform rainfall.

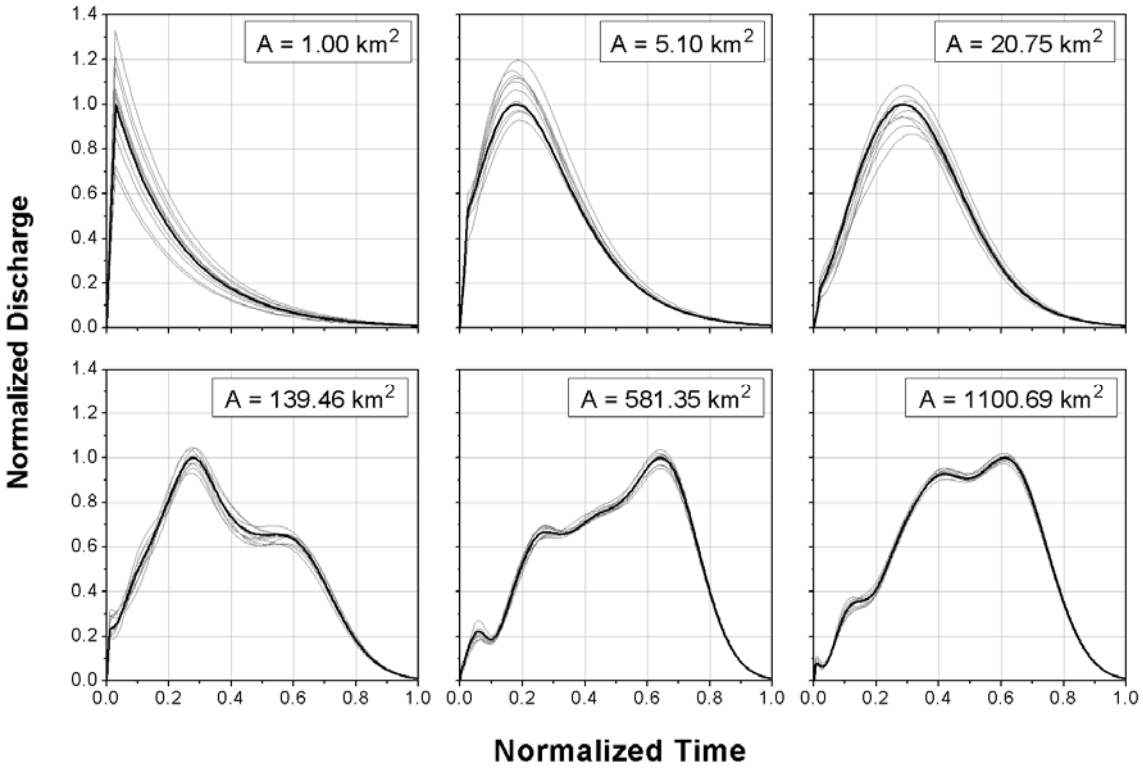

Figure 5: Hydrographs at six locations in the Whitewater River basin obtained from a distributed hydrologic model. The gray lines are the hydrographs for each of the 10 rainfall realizations assumed to be random in space, with the intensities following the uniform distribution U[20,100] mm/h for a duration of 10 minutes. The solid line represents hydrographs for the spatially uniform rainfall of 60 mm/h for 10 minutes.

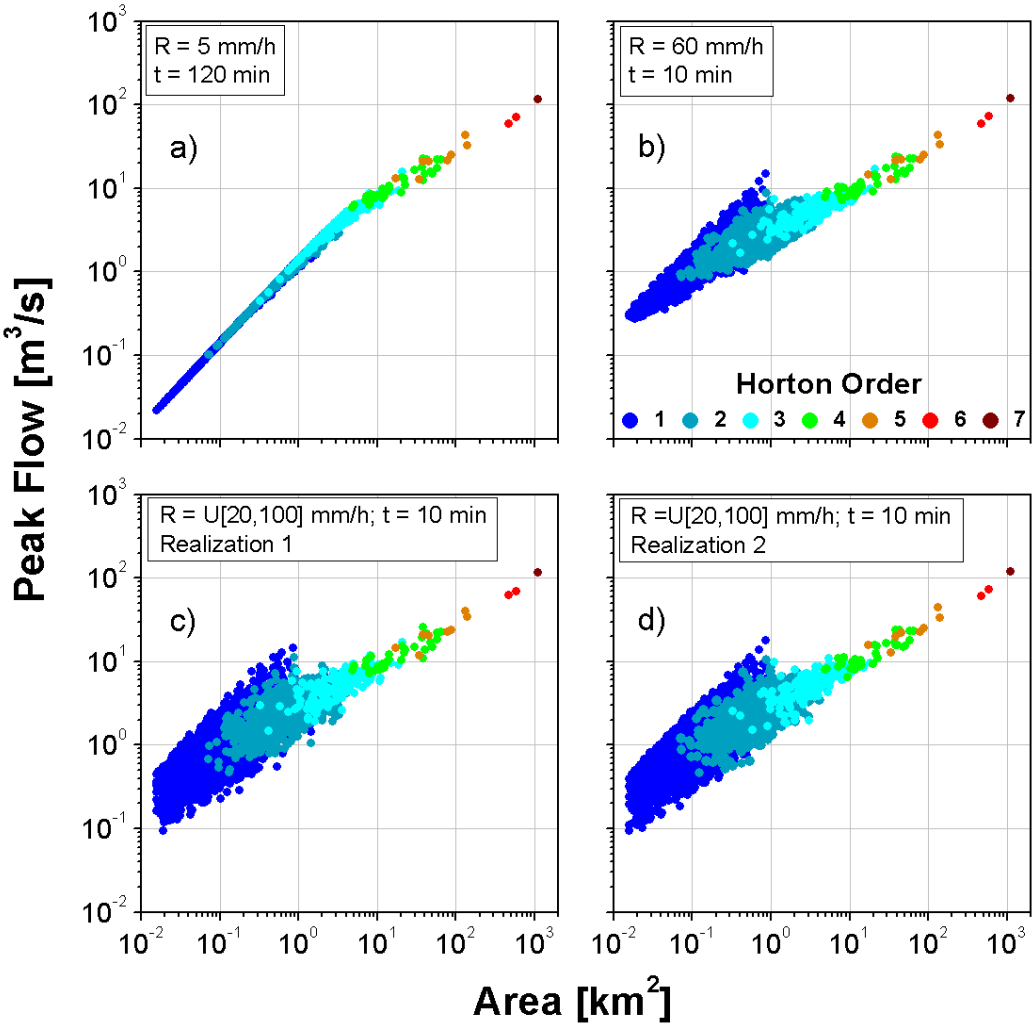

Figure 6: Scaling of peak flows with respect to the upstream areas of all the sub-basins in the Whitewater River basin. For (a) and (b), the rainfall is spatially uniform with the intensity and duration indicated on the panels. For (c) and (d), the rainfall is random in space with the intensities following the uniform distribution U[20,100] mm/h, and the duration is equal to 10 minutes.

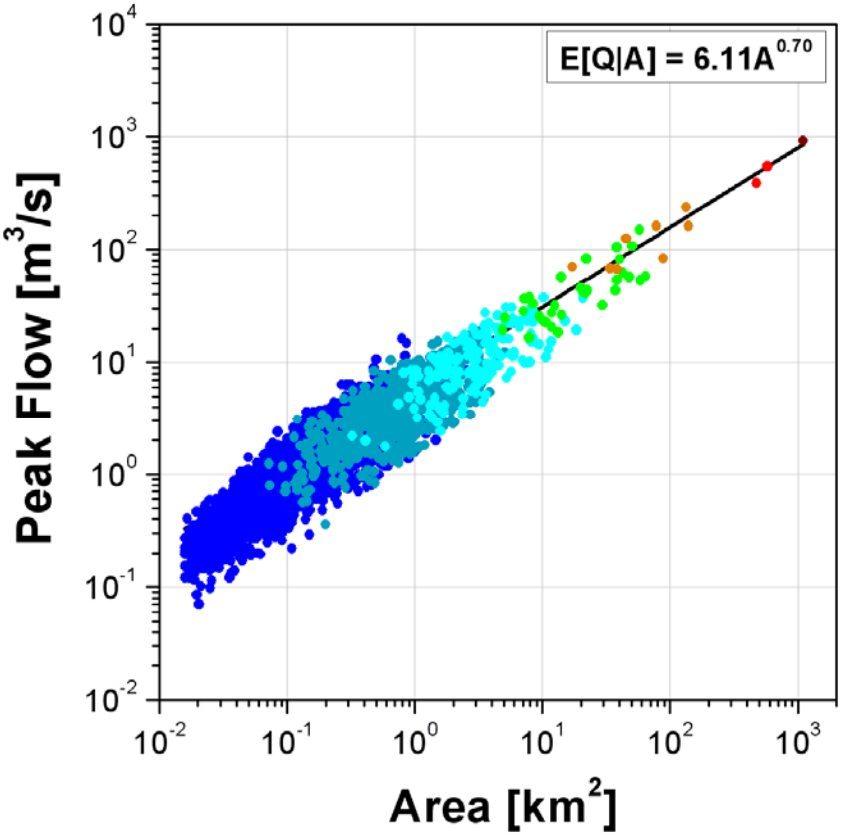

Figure 7: Scaling of the peak flows with respect to the upstream areas of all the sub-basins in the Whitewater River basin, Kansas. The rainfall data is obtained from the KICT NEXRAD weather radar in Wichita, Kansas. The color scheme indicates the Horton orders as in Figure 6.

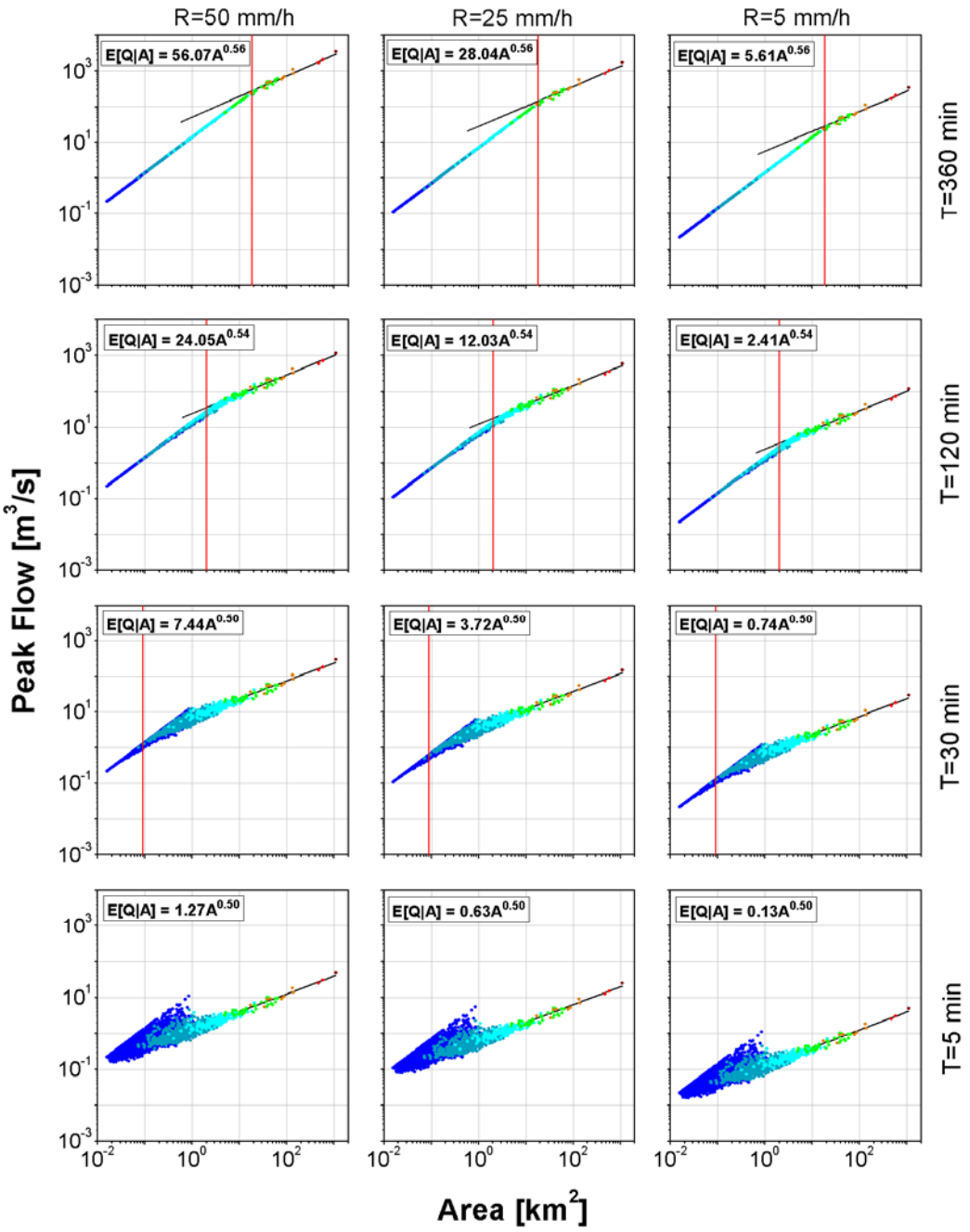

Figure 8: Sensitivity of the peak flow scaling structure to the intensity and duration of spatially uniform rainfall and linear channel routing with a velocity of 0.5 m/s. The solid black line represents the ordinary least squares fit (equation on each panel) obtained in the Hortonian framework. The solid red line indicates the scale break.

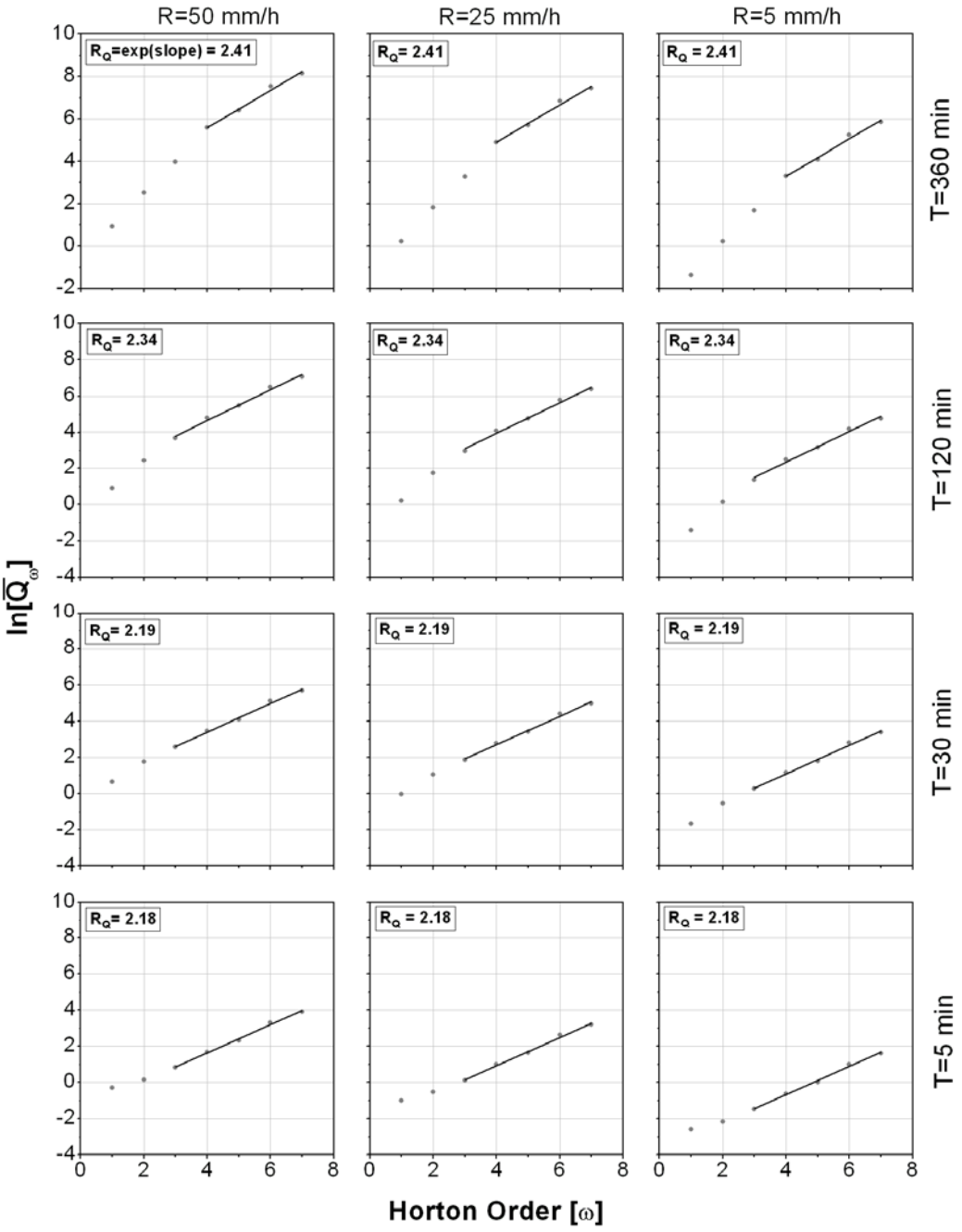

Figure 9: Horton plots of the peak flows for different combinations of intensity and duration of spatially uniform rainfall applied throughout the basin. The solid line indicates the ordinary least squares regression fit. The corresponding Horton ratios are also indicated on each panel.

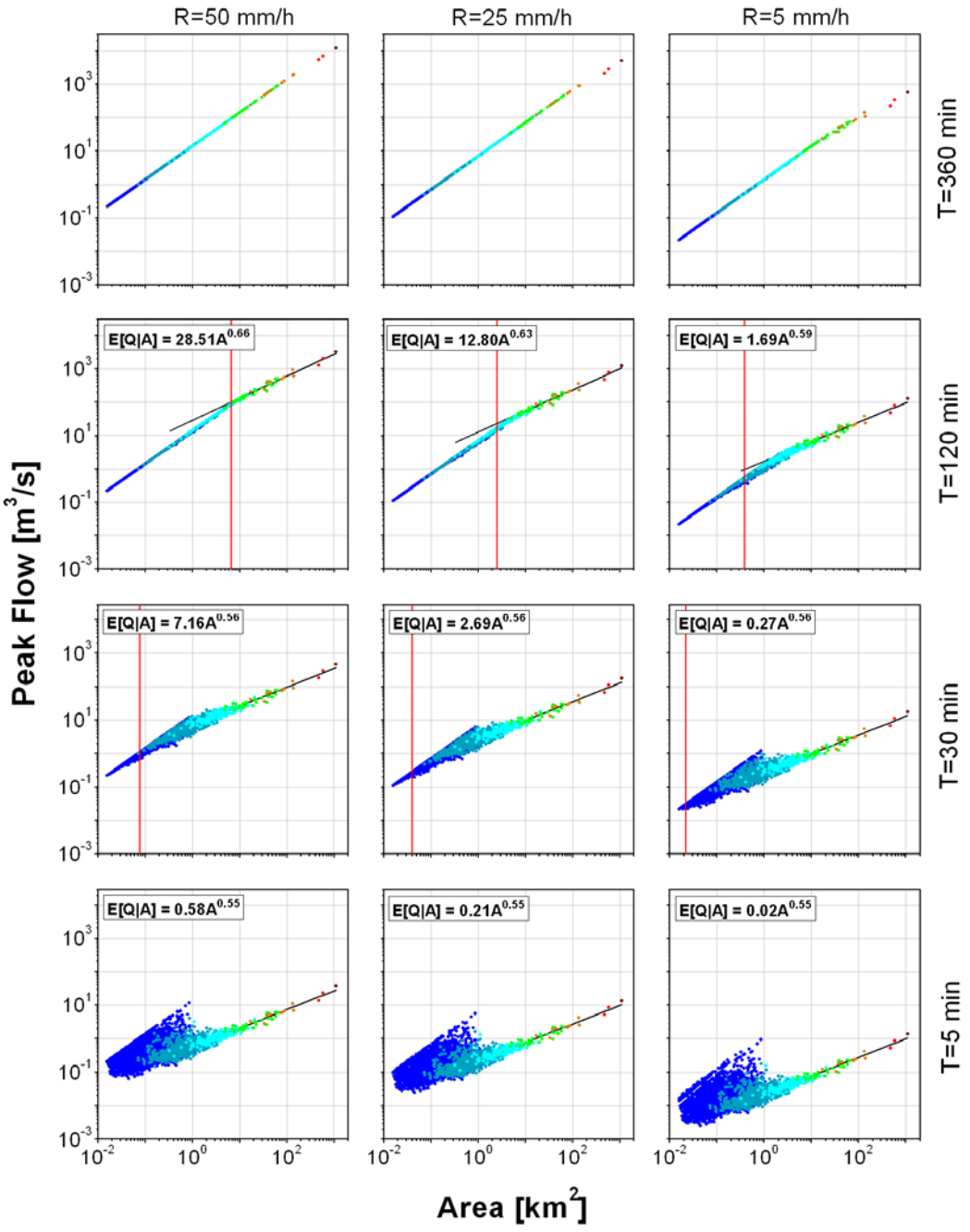

Figure 10: Sensitivity of the peak flow scaling structure to the intensity and duration of spatially uniform rainfall and nonlinear channel routing. The solid black line represents the ordinary least squares fit (equation on each panel) performed in the Hortonian framework. The solid red line indicates the scale break.

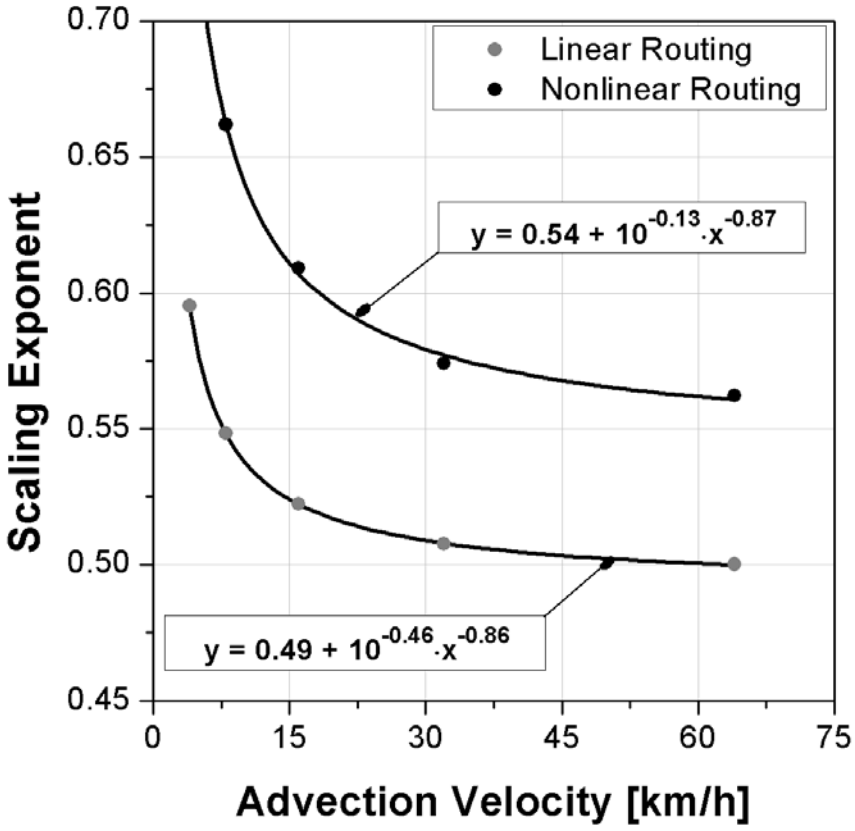

Figure 11: Sensitivity of the scaling exponent of peak flows to the advection velocity of spatially uniform rainfall of intensity 30 mm/h and linear and nonlinear channel routing mechanisms.

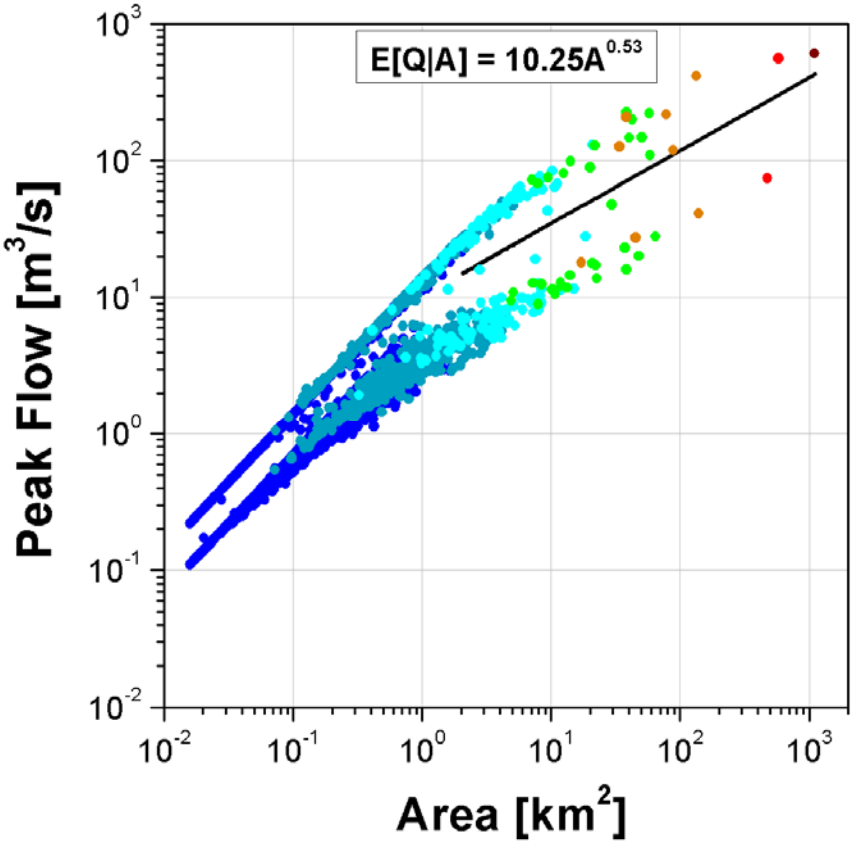

Figure 12: Effect of space-time variability of rainfall on the peak flow scaling structure. The rainfall is taken to be spatially uniform with an intensity of 25 mm/h for 30 minutes over the western half of the basin. For the eastern half of the basin, the rainfall is 50 mm/h for 120 minutes.

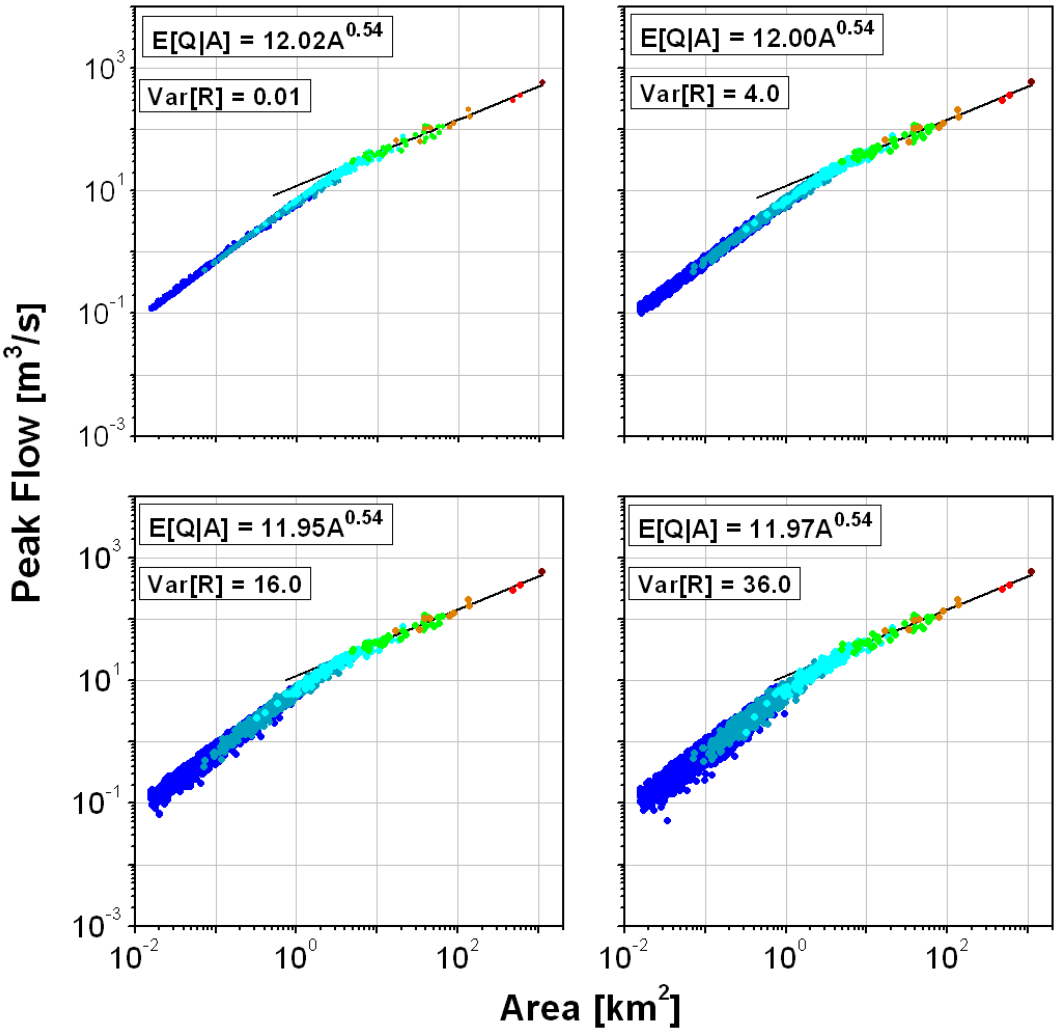

Figure 13: Sensitivity of the peak flow scaling structure to the variance of the rainfall field. The rainfall field is assumed to be Gaussian with a mean of 25 mm/h and variance indicated on each panel.

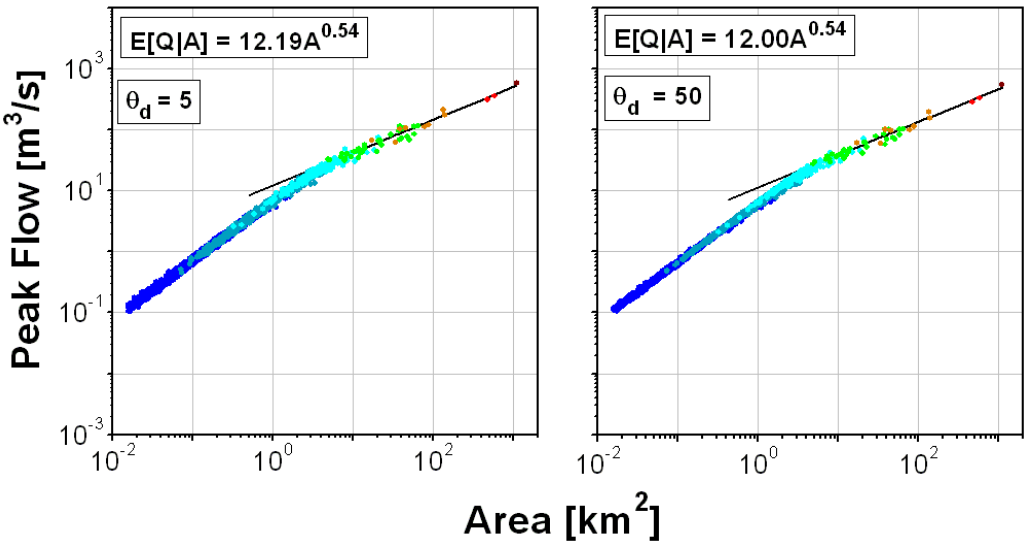

Figure 14: Sensitivity of the peak flow scaling structure to the spatial correlation of the rainfall field. The rainfall field is assumed to be Gaussian with a mean of 25 mm/h and a standard deviation of 2.0 mm/h. The spatial structure of the rainfall field is characterized by an exponential correlation structure with the correlation distance indicated on each panel.

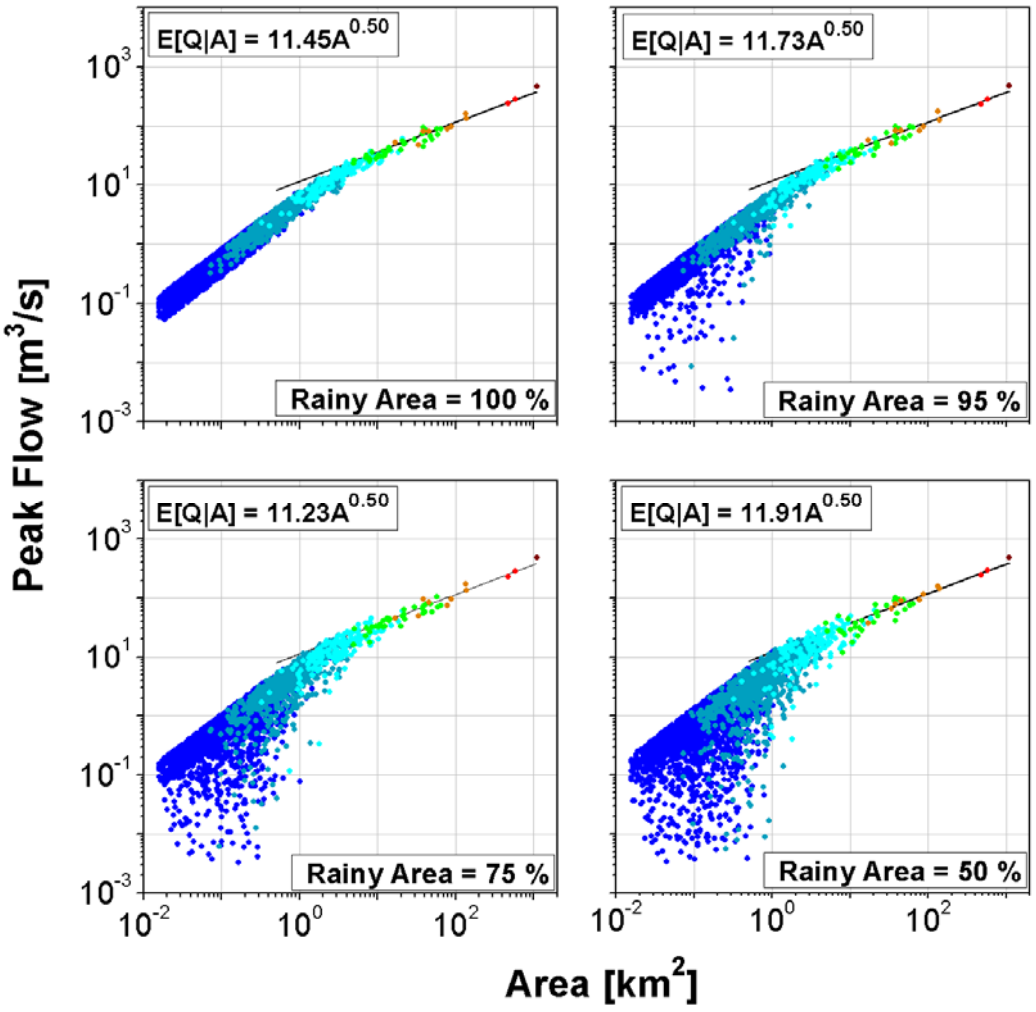

Figure 15: Sensitivity of the peak flow scaling structure to the zero-rainfall intermittency in rainfall fields. The rainfall fields are distributed randomly in space with the value at each pixel drawn from uniform distribution U[10,30] with a mean of 20 mm/h and a duration of 120 minutes.

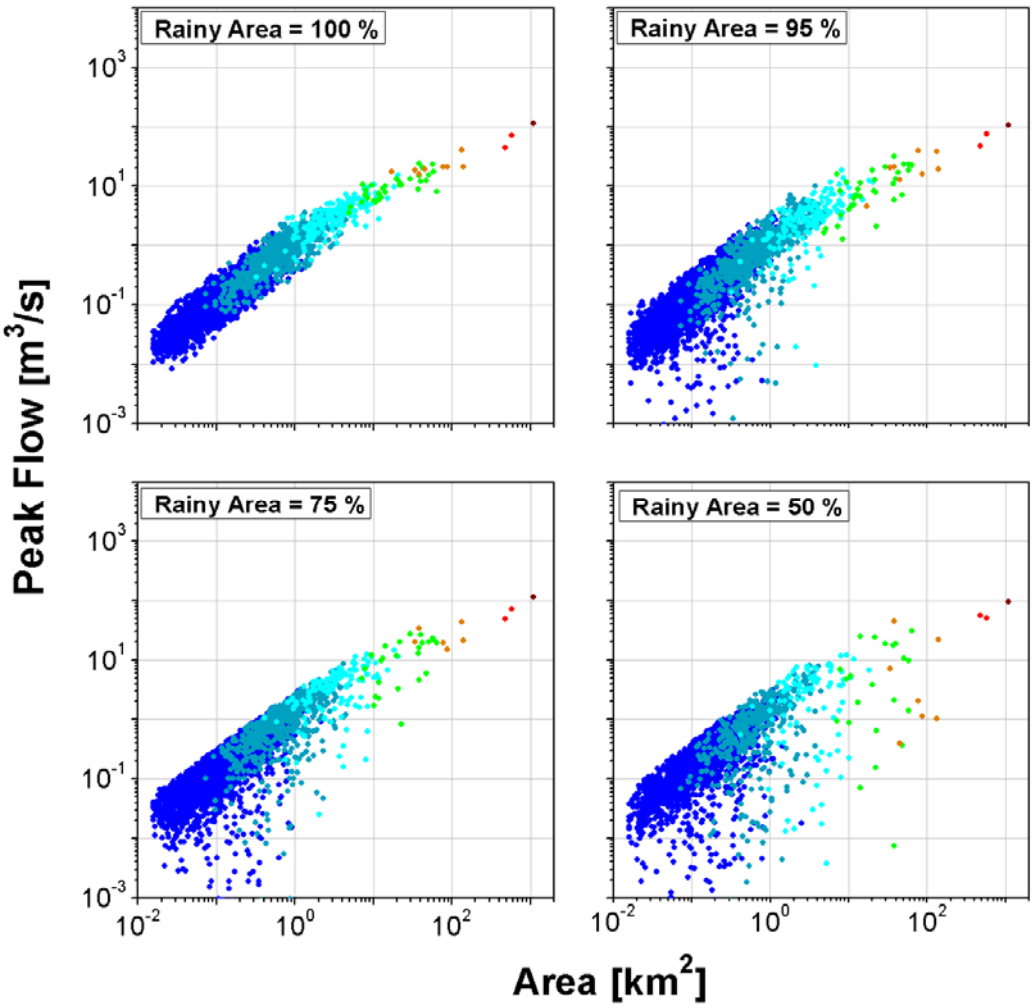

Figure 16: Sensitivity of the peak flow scaling structure to the spatial intermittency of rainfall field. The rainy portion of the field is assumed to follow a lognormal distribution. We did not show the regression equations as the peak flow scaling structure is too noisy to perform Hortonian regression for the bottom two panels of the Figure.

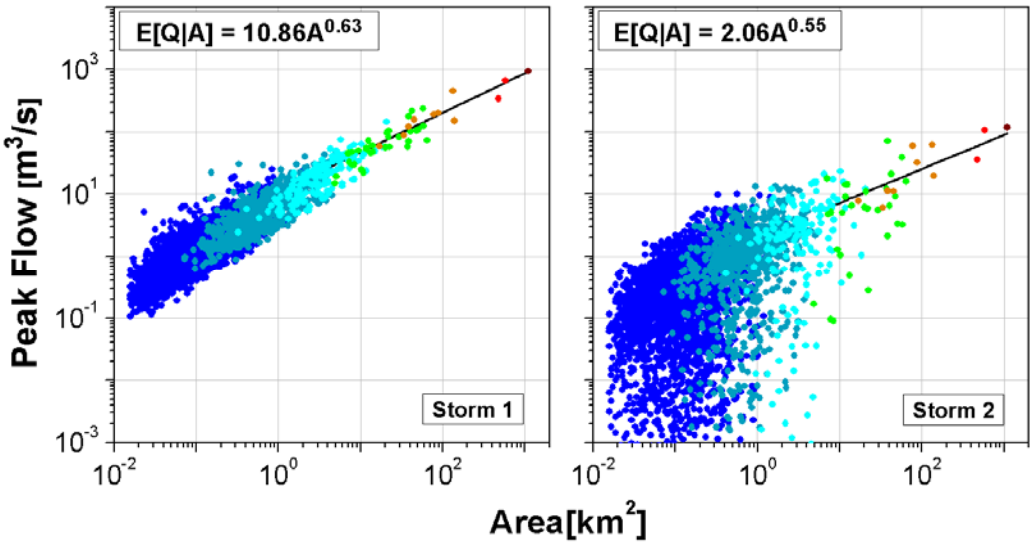

Figure 17: Response of the watershed to the simulated space-time rainfall events. The characteristics of the storms are listed in Table 3.

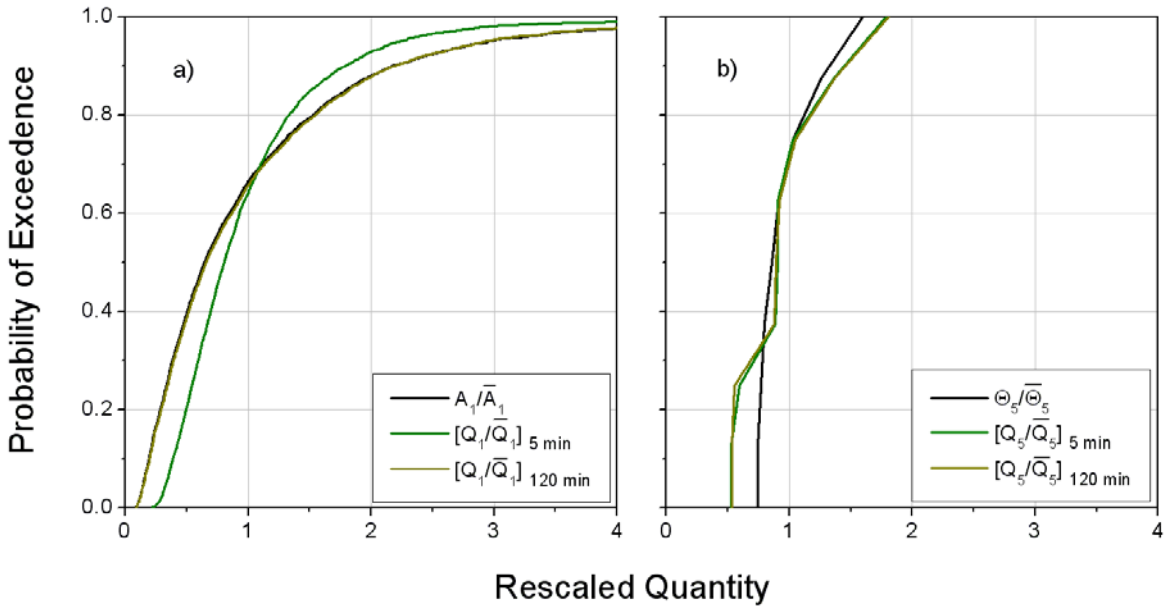

Figure 18: Probability distributions of rescaled areas, width function maxima and peak flows for order 1 and order 5 basins.